J|A|C|S
ARTICLES
Published on Web 01/31/2007

Tuning the Electrocrystallization Parameters of Semiconducting $Co[TCNQ]_2$-Based Materials To Yield either Single Nanowires or Crystalline Thin Films

Ayman Nafady,[†] Alan M. Bond,*[,†] Alexander Bilyk,[‡] Alexander R. Harris,[†] Anand I. Bhatt,[†] Anthony P. O'Mullane,[†] and Roland De Marco[§]

Contribution from the School of Chemistry, Monash University, P.O. Box 23, Victoria 3800, Australia, CSIRO Manufacturing & Materials Technology, P.O. Box 56 (Graham Road), Highett, Victoria 3190, Australia, and Department of Applied Chemistry, Curtin University of Technology, G.P.O. Box U 1987, Perth, Western Australia 6845, Australia

Received October 13, 2006; E-mail: Alan.Bond@sci.monash.edu.au

Abstract: Electrocrystallization of single nanowires and/or crystalline thin films of the semiconducting and magnetic $Co[TCNQ]_2(H_2O)_2$ (TCNQ = tetracyanoquinodimethane) charge-transfer complex onto glassy carbon, indium tin oxide, or metallic electrodes occurs when TCNQ is reduced in acetonitrile (0.1 M $[NBu_4][ClO_4]$) in the presence of hydrated cobalt(II) salts. The morphology of the deposited solid is potential dependent. Other factors influencing the electrocrystallization process include deposition time, concentration, and identity of the $Co^{2+}{}_{(MeCN)}$ counteranion. Mechanistic details have been elucidated by use of cyclic voltammetry, chronoamperometry, electrochemical quartz crystal microbalance, and galvanostatic methods together with spectroscopic and microscopic techniques. The results provide direct evidence that electrocrystallization takes place through two distinctly different, potential-dependent mechanisms, with progressive nucleation and 3-D growth being controlled by the generation of $[TCNQ]^{\bullet-}$ at the electrode and the diffusion of $Co^{2+}{}_{(MeCN)}$ from the bulk solution. Images obtained by scanning electron microscopy reveal that electrocrystallization of $Co[TCNQ]_2(H_2O)_2$ at potentials in the range of 0.1−0 V vs Ag/AgCl, corresponding to the $[TCNQ]^{0/\bullet-}$ diffusion-controlled regime, gives rise to arrays of well-separated, needle-shaped nanowires via the overall reaction $2[TCNQ]^{\bullet-}{}_{(MeCN)} + Co^{2+}{}_{(MeCN)} + 2H_2O \rightleftharpoons \{Co[TCNQ]_2(H_2O)_2\}_{(s)}$. In this potential region, nucleation and growth occur at randomly separated defect sites on the electrode surface. In contrast, at more negative potentials, a compact film of densely packed, uniformly oriented, hexagonal-shaped nanorods is formed. This is achieved at a substantially increased number of nucleation sites created by direct reduction of a thin film of what is proposed to be cobalt-stabilized $\{(Co^{2+})([TCNQ_2]^{\bullet-})_2\}$ dimeric anion. Despite the potential-dependent morphology of the electrocrystallized $Co[TCNQ]_2(H_2O)_2$ and the markedly different nucleation−growth mechanisms, IR, Raman, elemental, and thermogravimetric analyses, together with X-ray diffraction, all confirmed the formation of a highly pure and crystalline phase of $Co[TCNQ]_2(H_2O)_2$ on the electrode surface. Thus, differences in the electrodeposited material are confined to morphology and not to phase or composition differences. This study highlights the importance of the electrocrystallization approach in constructing and precisely controlling the morphology and stoichiometry of $Co[TCNQ]_2$-based materials.

Introduction

Metal−organic charge-transfer salts, network polymers, and organometallic compounds based on tetracyanoquinodimethane (TCNQ) frequently exhibit novel conducting and/or magnetic properties.[1] For this reason, TCNQ solid-state chemistry represents an area of considerable current interest in the field of materials science.[2] Potential applications of the fundamentally intriguing properties of these materials in optical and electrical media recording,[3] energy and data storage,[4] and sensors and catalysis,[5] as well as electrochromic and magnetic devices,[6] have been a driving force for the tremendous research activity over the past four decades. For example, the discovery of reversible bistable electrical and optical switches together with

(1) For examples, see: (a) LeBlanc, O. H., Jr. *J. Chem. Phys.* **1965**, *42*, 4307. (b) Torrance, J. B.; Scott, B. A.; Kaufman, F. B. *Solid State Commun.* **1975**, *17*, 1369. (c) Inoue, M. B.; Inoue, M.; Fernando, Q.; Nebesny, K. W. *J. Phys. Chem.* **1987**, *91*, 527. (d) Miller, J. S.; Calabrese, J. C.; Harlow, R. L.; Dixon, D. A.; Zhang, J. H.; Reiff, W. M.; Chittipeddi, S.; Selover, M. A.; Epstein, A. J. *J. Am. Chem. Soc.* **1990**, *112*, 5496. (e) Kaim, W.; Moscherosch, M. *Coord. Chem. Rev.* **1994**, *129*, 157. (f) Azcondo, M. T.; Ballester, L.; Golhen, S.; Gutierrez, A.; Ouahab, L.; Yartsev, S.; Delhaes, P. *J. Mater. Chem.* **1999**, *9*, 1237. (g) Kuroda, N.; Sugimoto, T.; Hagiwara, M.; Hasanudin; Ueda, K.; Tada, T.; Uozaki, H.; Toyota, N.; Mogi, I.; Watanabe, K.; Motokawa, M. *Synth. Met.* **2003**, *133/134*, 535. (h) Vickers, E. B.; Selby, T. D.; Thorum, M. S.; Taliaferro, M. L.; Miller, J. S. *Inorg. Chem.* **2004**, *43*, 6414. (i) Ueda, K.; Takahashi, M.; Tomizawa, H.; Miki, E.; Faulmann, C. *J. Mol. Struct.* **2005**, *751*, 12. (j) Taliaferro, M. L.; Palacio, F.; Miller, J. S. *J. Mater. Chem.* **2006**, *16*, 2677. (k) Miyasaka, H.; Izawa, T.; Takahashi, N.; Yamashita, M.; Dunbar, K. R. *J. Am. Chem. Soc.* **2006**, *128*, 11358. (l) Mikuriya, M.; Yoshioka, D.; Handa, M. *Coord. Chem. Rev.* **2006**, *250*, 2194.

[†] Monash University.
[‡] CSIRO Manufacturing & Materials Technology.
[§] Curtin University of Technology.

10.1021/ja067219j CCC: $37.00

memory effects for both CuTCNQ and AgTCNQ based devices has substantially encouraged exploration of new approaches for achieving precise control of the physical (e.g., shape, size, density, orientation) and chemical (phase, structure, purity) properties of these materials.[7] These methods include the use of the spontaneous electrolysis technique (reaction of dissolved TCNQ in acetonitrile with metallic copper or silver), electrospinning of a mixture of TCNQ and metal salts dissolved in an appropriate polymer solution, and vapor deposition of TCNQ on metal surfaces.[8]

Significant contributions in these endeavors to design and fabricate molecular ions into high-quality crystalline materials have been accomplished by use of electrocrystallization.[9] In the case of CuTCNQ[10] and other 1:1 metal−TCNQ charge-transfer materials,[11] such studies have significantly enhanced the understanding of the factors and mechanisms that control the nucleation and growth processes, as well as the role of phase, morphology, and stoichiometry in determining the electronic and conducting properties of these materials. In stark contrast, knowledge concerning the conceptually related semiconducting binary $M[TCNQ]_2$-based materials (where M is a first-row transition metal), since their initial discovery by Melby and coworkers in 1962, is rudimentary.[12] Nonetheless, renewed interest in this class of material has emerged since Dunbar et al. synthesized $M[TCNQ]_2(S)_2$ complexes (M = Mn, Fe, Co, Ni; S = H_2O or MeOH) as network polymers with diverse magnetic properties.[13] This group[14] and Miller et al.[15] subsequently reported synthetic methodolgies based on the use of highly reactive precursors such as $[M(MeCN)_6][BF_4]_2$, $[M(MeCN)_6][SbF_6]_2$, or metal carbonyls $M_a(CO)_b$, along with ultrapure solvents and inert atmospheres, for the preparation of solvent-free "glassy magnets"[14] or molecular magnets[15] of the $M[TCNQ]_2$ family. A major synthetic impediment apparent in these reports is imposed by the rapid precipitation of $M[TCNQ]_2$ (M = Mn, Fe, Co, Ni) products, which, in most cases, leads to formation of either impure or amorphous materials. These and other related problems[16] have thwarted research efforts to achieve comprehensive evaluations of the magnetic and structure−function correlations of these materials.

A sparsely investigated avenue for the synthesis and characterization of $M[TCNQ]_2$-based materials, and of particular interest in this paper, is the use of electrochemical techniques.[17] In a recent publication,[18] we have described the electrochemical formation and characterization of needle-shaped crystals of $Co[TCNQ]_2(H_2O)_2$ through the redox-based solid−solid transformation of microcrystalline TCNQ solid adhered to an electrode in contact with aqueous media containing $Co^{2+}_{(aq)}$ ions. In view of the recent high demand for controllable synthesis/growth as

(2) (a) Arena, A.; Patane, S.; Saitta, G.; Bonavita, A. *Mater. Lett.* **2006**, *60*, 2171. (b) Kaur, P.; Sarangal, A.; Hundal, G.; McInnes, E. *J. Coord. Chem.* **2006**, *59*, 821. (c) Lu, J.; Nagase, S.; Zhang, X.; Wang, D.; Ni, M.; Maeda, Y.; Wakahara, T.; Nakahodo, T.; Tsuchiya, T.; Akasaka, T.; Gao, Z.; Yu, D.; Ye, H.; Mei, W. N.; Zhou, Y. *J. Am. Chem. Soc.* **2006**, *128*, 5114. (d) Morita, Y.; Miyazaki, E.; Umemoto, Y.; Fukui, K.; Nakasuji, K. *J. Org. Chem.* **2006**, *71*, 5631. (e) Tsiperman, E.; Becker, J. Y.; Khodorkovsky, V.; Shames, A.; Shapiro, L. *Angew. Chem., Int. Ed.* **2005**, *44*, 4015. (f) Hibbs, W.; Arif, A. M.; Botoshansky, M.; Kaftory, M.; Miller, J. S. *Inorg. Chem.* **2003**, *42*, 2311. (g) Pokhodnya, K. I.; Petersen, N.; Miller, J. S. *Inorg. Chem.* **2002**, *41*, 1996. (h) Miyasaka, H.; Campos-Fernandez, C. S.; Clerac, R.; Dunbar, K. R. *Angew. Chem., Int. Ed.* **2000**, *39*, 3831. (i) Higo, M.; Lu, X.; Mazur, U.; Hipps, K. W. *Chem. Lett.* **1999**, 679.

(3) (a) Mo, X.-L.; Chen, G.-R.; Cai, Q.-J.; Fan, Z.-Y.; Xu, H.-H.; Yao, Y.; Yang, J.; Gu, H.-H.; Hua, Z.-Y. *Thin Solid Films* **2003**, *436*, 259. (b) Yamaguchi, S.; Potember, R. S. *Synth. Met.* **1996**, *78*, 117. (c) Kim, J.; Cho, O.; Min, K.; Park, K. *Synth. Met.* **1995**, *71*, 2215. (d) Cho, O. K.; Park, K. Y. *Mol. Cryst. Liq. Cryst.* **1995**, *267*, 393.

(4) (a) Ran, C.; Peng, H.; Zhou, W.; Yu, X.; Liu, Z. *J. Phys. Chem. B* **2005**, *109*, 22486. (b) Peng, H.; Chen, Z.; Tong, L.; Yu, X.; Ran, C.; Liu, Z. *J. Phys. Chem. B* **2005**, *109*, 3526. (c) Fan, Z. Y.; Mo, X. L.; Chen, G. R.; Lu, J. G. *Rev. Adv. Mater. Sci.* **2003**, *5*, 72.

(5) (a) Luz, R. d. C. S.; Damos, F. S.; Bof de Oliveira, A.; Beck, J.; Kubota, L. T. *Sens. Actuators B* **2006**, *B117*, 274. (b) Cano, M.; Palenzuela, B.; Rodriguez-Amaro, R. *Electroanalysis* **2006**, *18*, 1068. (c) Llopis, X.; Merkoci, A.; del Valle, M.; Alegret, S. *Sens. Actuators B* **2005**, *B107*, 742. (d) Wooster, T. J.; Bond, A. M. *Analyst* **2003**, *128*, 1386. (e) Pandey, P. C.; Upadhyay, S.; Sharma, S. *Electroanalysis* **2003**, *15*, 1115. (f) Palmisano, F.; Zambonin, P. G.; Centonze, D.; Quinto, M. *Anal. Chem.* **2002**, *74*, 5913. (g) Winkler, K.; Plonska, M. E.; Basa, A.; Lach, M.; Balch, A. L. *Electroanalysis* **2002**, *15*, 55. (h) Cheng, Y.; Schiffrin, D. J. *J. Chem. Soc., Faraday Trans.* **1994**, *90*, 2517. (i) Freund, M. S.; Brajter-Toth, A.; Ward, M. D. *J. Electroanal. Chem.* **1990**, *289*, 127. (j) Sharp, M. *Anal. Chim. Acta* **1976**, *85*, 17.

(6) (a) Perepichka, D. F.; Bryce, M. R.; Pearson, C.; Petty, M. C.; McInnes, E. J. L.; Zhao, J. P. *Angew. Chem., Int. Ed.* **2003**, *42*, 4636. (b) Yasuda, A.; Seto, J. *J. Electroanal. Chem.* **1988**, *247*, 193. (c) Valade, L.; de Caro, D.; Malfant, I. *NATO Sci. Series II: Math. Phys. Chem.* **2004**, *139*, 241.

(7) (a) Potember, R. S.; Poehler, T. O.; Cowan, D. O. *Appl. Phys. Lett.* **1979**, *34*, 405. (b) Potember, R. S.; Poehler, T. O.; Benson, R. C. *Appl. Phys. Lett.* **1982**, *41*, 548. (c) Kamitsos, E. I.; Risen, J. W. M. *Solid State Commun.* **1983**, *45*, 165. (d) Poehler, T. O.; Potember, R. S.; Hoffman, R.; Benson, R. C. *Mol. Cryst. Liq. Cryst.* **1984**, *107*, 91. (e) Hoagland, J. J.; Wang, X. D.; Hipps, K. W. *Chem. Mater.* **1993**, *5*, 54. (f) Gu, N.; Yang, X.-M.; Sheng, H.-Y.; Lu, W.; Wei, Y. *Synth. Met.* **1995**, *71*, 2221. (g) Liu, S.-G.; Liu, Y.-Q.; Wu, P.-J.; Zhu, D.-B.; Tien, H.; Chen, K.-C. *Thin Solid Films* **1996**, *289*, 300. (h) Sun, S.; Wu, P.; Zhu, D. *Thin Solid Films* **1997**, *301*, 192. (i) Sun, S.; Xu, X.; Wu, P.; Zhu, D. *J. Mater. Sci. Lett.* **1998**, *17*, 719. (j) Oyamada, T.; Tanaka, H.; Matsushige, K.; Sasabe, H.; Adachi, C. *Appl. Phys. Lett.* **2003**, *83*, 1252. (k) Fan, Z. Y.; Mo, X. L.; Chen, G. R.; Lu, J. G. *Rev. Adv. Mater. Sci.* **2003**, *5*, 72. (l) Fan, Z. Y.; Mo, X. L.; Lou, C. F.; Yao, Y.; Wang, D. W.; Chen, G. R.; Lu, J. G. *IEEE Trans. Nanotech.* **2005**, *4*, 238. (m) Muller, R.; Genoe, J.; Heremans, P. *Appl. Phys. Lett.* **2006**, *88*, 242105.

(8) (a) Torrance, J. B. *Acc. Chem. Res.* **1979**, *12*, 79. (b) Gu, Z.; Wu, H.; Wei, Y.; Liu, J. *J. Phys. Chem.* **1993**, *97*, 2543. (c) Yuan, C.-W.; Lu, W.; Chen, C.-Y.; Wei, Y. *Synth. Met.* **1993**, *59*, 235. (d) Wachtel, H.; Ferger, J.; von Schutz, J. U.; Wolf, H. C. *Synth. Met.* **1995**, *71*, 2103. (e) Heintz, R. A.; Zhao, H.; Ouyang, X.; Grandinetti, G.; Cowen, J.; Dunbar, K. R. *Inorg. Chem.* **1999**, *38*, 144. (f) O'Kane, S. A.; Clerac, R.; Zhao, H.; Ouyang, X.; Galan-Mascaros, J. R.; Heintz, R.; Dunbar, K. R. *J. Solid-State Chem.* **2000**, *152*, 159. (g) Zhang, Q.; Wang, W.; Ye, G.; Yan, X.; Zhang, Z.; Hua, Z. *Synth. Met.* **2004**, *144*, 285. (h) Liu, H.; Zhao, Q.; Li, Y.; Liu, Y.; Lu, F.; Zhuang, J.; Wang, S.; Jiang, L.; Zhu, D.; Yu, D.; Chi, L. *J. Am. Chem. Soc.* **2005**, *127*, 1120. (i) Liu, Y.; Ji, Z.; Tang, Q.; Jiang, L.; Li, H.; He, M.; Hu, W.; Zhang, D.; Jiang, L.; Wang, X.; Wang, C.; Liu, Y.; Zhu, D. *Adv. Mater.* **2005**, *17*, 2953. (j) Cao, G.; Fang, F.; Ye, C.; Xing, X.; Xu, H.; Sun, D.; Chen, G. *Micron* **2005**, *36*, 285. (k) Cao, G.; Ye, C.; Fang, F.; Xing, X.; Xu, H.; Sun, D.; Chen, G. *Micron* **2005**, *36*, 267. (l) Muller, R.; De Jonge, S.; Myny, K.; Wouters, D. J.; Genoe, J.; Heremans, P. *Solid-State Electron.* **2006**, *50*, 601.

(9) (a) Kathirgamanathan, P.; Mucklejohn, S. A.; Rosseinsky, D. R. *J. Chem. Soc., Chem. Commun.* **1979**, 86. (b) Ward, M. D. *Inorg. Chem.* **1986**, *25*, 4444. (c) Ward, M. D.; Johnson, D. C. *Inorg. Chem.* **1987**, *26*, 4213. (d) Ward, M. D. *Synth. Met.* **1988**, *27*, B211. (e) Batail, P.; Boubekeur, K.; Fourmigue, M.; Gabriel, J.-C. P. *Chem. Mater.* **1998**, *10*, 3005. (f) Legros, J.-P.; Dahan, F.; Binet, L.; Carcel, C.; Fabre, J.-M. *J. Mater. Chem.* **2000**, *10*, 2685.

(10) (a) Neufeld, A. K.; Madsen, I.; Bond, A. M.; Hogan, C. F. *Chem. Mater.* **2003**, *15*, 3573. (b) Neufeld, A. K.; O'Mullane, A. P.; Bond, A. M. *J. Am. Chem. Soc.* **2005**, *127*, 13846. (c) Harris, A. R.; Neufeld, A. K.; O'Mullane, A. P.; Bond, A. M.; Morrison, R. J. S. *J. Electrochem. Soc.* **2005**, *152*, C577. (d) O'Mullane, A. P.; Neufeld, A. K.; Harris, A. R.; Bond, A. M. *Langmuir* **2006**, *22*, 10499. (e) Harris, A. R.; Neufeld, A. K.; O'Mullane, A. P.; Bond, A. M. *J. Mater. Chem.* **2006**, *16*, 4397.

(11) (a) Bond, A. M.; Fletcher, S.; Marken, F.; Shaw, S. J.; Symons, P. G. *J. Chem. Soc., Faraday Trans.* **1996**, *92*, 3925. (b) Bond, A. M.; Fletcher, S.; Symons, P. G. *Analyst* **1998**, *123*, 1891. (c) Suarez, M. F.; Bond, A. M.; Compton, R. G. *J. Solid State Electrochem.* **1999**, *4*, 24. (d) Gomez, L.; Rodriguez-Amaro, R. *Langmuir* **2006**, *22*, 7431.

(12) (a) Melby, L. R.; Harder, R. J.; Hertler, W. R.; Mahler, W.; Benson, R. E.; Mochel, W. E. *J. Am. Chem. Soc.* **1962**, *84*, 3374.

(13) (a) Zhao, H.; Heintz, R. A.; Dunbar, K. R.; Rogers, R. D. *J. Am. Chem. Soc.* **1996**, *118*, 12844. (b) Zhao, H.; Heintz, R. A.; Ouyang, X.; Dunbar, K. R.; Campana, C. F.; Rogers, R. D. *Chem. Mater.* **1999**, *11*, 736. (c) Zhao, H.; Heintz, R. A.; Ouyang, X.; Grandinetti, G.; Cowen, J.; Dunbar, K. R. *NATO ASI Ser. Ser. C* **1999**, *518*, 353.

(14) Clerac, R.; O'Kane, S.; Cowen, J.; Ouyang, X.; Heintz, R.; Zhao, H.; Bazile, M. J., Jr.; Dunbar, K. R. *Chem. Mater.* **2003**, *15*, 1840.

(15) Vickers, E. B.; Giles, I. D.; Miller, J. S. *Chem. Mater.* **2005**, *17*, 1667.

(16) Although these materials are almost insoluble in most organic solvents, they exhibit some solubility in alcohols (MeOH) and water when converted into their solvated phases.

(17) (a) Siedle, A. R.; Candela, G. A.; Finnegan, T. F. *Inorg. Chim. Acta* **1979**, *35*, 125. (b) Kathirgamanathan, P.; Rosseinsky, D. R. *J. Chem. Soc., Chem. Commun.* **1980**, 839.

(18) Nafady, A.; O'Mullane, A. P.; Bond, A. M.; Neufeld, A. K. *Chem. Mater.* **2006**, *18*, 4375.

well as fabrication of materials that exhibit magnetic and/or conducting properties for nanoelectronic devices,[19] we now describe a facile and reproducible approach, along with new mechanistic insights, for the electrocrystallization of Co[TCNQ]$_2$(H_2O)$_2$ onto carbon, metal, and semiconducting electrode surfaces from acetonitrile (0.1 M [NBu_4][ClO_4]) solutions containing both TCNQ and $Co^{2+}_{(MeCN)}$ ions. Factors potentially affecting the electrocrystallization process, such as deposition time and potential, concentration and ratio of both TCNQ and $Co^{2+}_{(MeCN)}$ ions, as well as the identity of the $Co^{2+}_{(MeCN)}$ counteranion, have been explored in detail. Importantly, this study demonstrates that (a) the electrocrystallization process occurs through two distinctly different, potential-dependent nucleation−growth mechanisms and (b) the morphology of the deposited Co[TCNQ]$_2$(H_2O)$_2$ solid can be easily manipulated to favor either a crystalline thin film or single nanowire crystals. Finally, the structure, composition, and crystallinity of the electrocrystallized Co[TCNQ]$_2$(H_2O)$_2$ have been confirmed via a wide range of spectroscopic and microscopic techniques.

Experimental Section

Materials. Hydrated $Co(ClO_4)_2$ and $Co(NO_3)_2$ (analytical reagent grade), TCNQ (98%) (Aldrich), and acetonitrile (HPLC, Omnisolv) were used as received from the suppliers. [NBu_4][ClO_4] was purchased from Aldrich, recrystallized several times from ethanol (95%), and vacuum-dried prior to use.

Electrochemistry. Electrochemical measurements were undertaken at 293 ± 2 K with an Autolab PGSTAT100 (ECO-Chemie) workstation and a standard three-electrode cell configuration. For voltammetric and galvanostatic experiments, glassy carbon (3 mm diameter, Bioanalytical Systems), gold (125 μm or 1.6 mm diameter, Bioanalytical Systems), platinum (1.6 mm diameter, Bioanalytical Systems), and indium tin oxide (ITO)-coated glass (0.06−0.1 cm^2 area, Prazisions Glas and Optik GmbH) having a 10 Ω/sq sheet resistance, as quoted by the manufacturer, were used as the working electrodes. The procedures employed for polishing these electrodes are described elsewhere.[18] The reference electrode was AgCl-coated Ag wire obtained via anodic electrolysis of the silver wire in 0.1 M KCl and separated from the test solution by a salt bridge containing acetonitrile (0.1 M [NBu_4][ClO_4]). The Ag/AgCl potential is −0.294 V versus the ferrocene/ferrocenium ($Fc^{0/+}$) scale. The auxiliary electrode was made of platinum mesh. Bulk electrolysis experiments used to establish the identity of the electrocrystallized material were conducted in an "H-type" three-compartment cell, in which the compartments were separated by fine frits to minimize mixing of the solutions. In this case, large-area platinum foil (1.5 × 1.0 cm) or a platinum basket was used as the working electrode.

Electrochemical quartz crystal microbalance (EQCM) experiments were conducted at a 5 mm diameter gold film electrode with an ELCHEMA EQCN-701 quartz crystal nanobalance and a PS-205 potentiostat connected to a computer via an Advantech PCI-1711 DAQ device. Other experimental details are as reported elsewhere.[10c]

Physical Measurements. Infrared spectroscopy (IR), scanning electron microscopy (SEM), energy-dispersive analysis of X-rays (EDAX), and conventional powder X-ray diffraction (XRD) experiments were carried out as previously described.[18] Ex situ synchrotron radiation−grazing incidence X-ray diffraction (SR-GIXRD) measurements of electrodeposited films of Co[TCNQ]$_2$-based material on ITO electrode surfaces were undertaken on beamline 20B at the Photon Factory in Tsukuba, Japan, using the "BIGDIFF" difractometer and an experimental rig that has been described elsewhere.[20] A nominal wavelength of 1.0 Å was used, and parallel beam optics provided an incident beam with dimensions of 100 μm and 2 mm in the vertical and horizontal directions, respectively. The ITO electrode diffraction pattern was used as an internal standard for calibration of the synchrotron beam wavelength, yielding an actual value of 0.976 Å. Grazing incidence X-ray diffraction (GIXRD) measurements were taken at angles of incidence between 0.1° and 5° using Fuji imaging plates and an exposure time of 20 min. A portable Princeton Applied Research PARSTAT 2263 potentiostat was transported to the Photon Factory and used along with a standard four-necked electrochemical cell equipped with an ITO working electrode, Ag/AgCl reference electrode, platinum mesh auxiliary electrodes, and a nitrogen inlet tube, to electrodeposit Co[TCNQ]$_2$-based materials via bulk electrolysis at short electrolysis times (2−4 min) with $E_{app} = -0.15$ V vs Ag/AgCl. The ex situ SR-GIXRD measurements on the electrocrystallized films were recorded under very low humidity (3 horsepower dehumidifier) inside the "BIGDIFF" diffractometer. In order to provide a simple comparison of the present SR-GIXRD results with the diffraction data reported by Dunbar et al.[13b,14] using a conventional laboratory-based diffractometer (Cu Kα; $\lambda = 1.5418$ Å), we have normalized the 2θ values to those that would have been obtained at $\lambda = 1.5418$ Å using Bragg's law of diffraction, viz. $n\lambda = 2d \sin\theta$, where n is the diffraction order, λ is the wavelength, d is the interplanar spacing, and θ is the diffraction angle. For example, the three preferred oriented diffraction planes observed at 2θ values of 5.25°, 10.50°, and 15.25° at $\lambda = 0.976$ Å, as observed using SR-GIXRD, yielded 2θ values of 8.30°, 16.62°, and 24.20° at $\lambda = 1.5418$ Å.

Electronic spectra were obtained with a Varian Cary 5 UV−visible spectrophotometer using a 1 cm path length cell (Varian OS2 software). Raman spectra were obtained with a Renishaw RM 2000 Raman spectrograph and microscope using a 18 mW, 780 nm excitation source. Thermogravimetric analysis (TGA) was achieved with a STA1500 instrument (Rheometric Scientific) in a nitrogen atmosphere between 30 and 400 °C with a rate of temperature change of 10 °C/min.

Results and Discussion

I. Probing the Electrocrystallization of Co[TCNQ]$_2$-Based Materials. A. Voltammetric Reduction of TCNQ in the Presence of $Co^{2+}_{(MeCN)}$ Ions.[21] Cyclic voltammetry was used to establish the potential needed to electrocrystallize Co[TCNQ]$_2$-based materials. Cyclic voltammograms obtained at a scan rate of 100 mV s^{-1} for the reduction of 1.0 mM TCNQ in the absence and in the presence of 0.5 mM $Co(ClO_4)_2$ ($Co^{2+}_{(MeCN)}$:TCNQ ratio of 1:2) in acetonitrile (0.1 M [NBu_4][ClO_4]) at a glassy carbon (GC) electrode are shown in Figure 1. In the absence of $Co^{2+}_{(MeCN)}$ ions (black curve, Figure 1), two well-separated, diffusion-controlled, one-electron, chemically and electrochemically reversible processes are observed at $E^\circ_1 = 0.170$ V and $E^\circ_2 = -0.380$ V vs Ag/AgCl.[22] These processes correspond to reduction of TCNQ to $[TCNQ]^{\bullet-}$ and $[TCNQ]^{2-}$, respectively, according to eqs 1 and 2. The potential separation ($\Delta E^\circ = E^\circ_1 - E^\circ_2 = 550$ mV) is in excellent

(19) (a) Xiao, K.; Ivanov, I. N.; Puretzky, A. A.; Liu, Z.; Geohegan, D. B. *Adv. Mater.* **2006**, *18*, 2184. (b) Shang, T.; Yang, F.; Zheng, W.; Wang, C. *Small* **2006**, *2*, 1007. (c) Liu, Y.; Li, H.; Tu, D.; Ji, Z.; Wang, C.; Tang, Q.; Liu, M.; Hu, W.; Liu, Y.; Zhu, D. *J. Am. Chem. Soc.* **2006**, *128*, 12917.

(20) (a) De Marco, R.; Pejcic, B.; Prince, K.; van Riessen, A. *Analyst* **2003**, *128*, 742. (b) De Marco, R.; Jiang, Z. T.; Pejcic, B.; Poinen, E. *J. Electrochem. Soc.* **2005**, *152*, B389. (c) De Marco, R.; Jiang, Z. T.; Pejcic, B.; van Riessen, A. *Electrochim. Acta* **2006**, *51*, 4886. (d) De Marco, R.; Jiang, Z. T.; Martizano, J.; Lowe, A.; Pejcic, B.; van Riessen, A. *Electrochim. Acta* **2006**, *51*, 5920.

(21) $Co^{2+}_{(MeCN)}$ precursor refers to the solvated $[Co(MeCN)_6]^{2+}$ complex formed as a result of dissolving hydrated Co(II) salts in acetonitrile.

(22) E° is the reversible formal potential calculated as the average of the reduction (E_p^{red}) and oxidation (E_p^{ox}) peak potentials obtained from cyclic voltammograms.

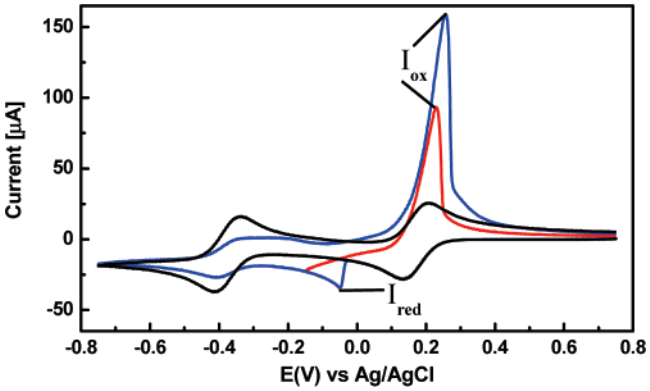

Figure 1. (a) Cyclic voltammograms obtained in acetonitrile (0.1 [NBu_4][ClO_4]) with a 3 mm diameter GC electrode and scan rate of 100 mV s^{-1} for the reduction of 1.0 mM TCNQ in the absence (black curve) and in the presence of 0.5 mM $Co(ClO_4)_2 \cdot 6H_2O$ at a 1:2 ratio and when the potential is switched before (red curve) and after (blue curve) the $[TCNQ]^{\bullet -/2-}$ reduction process.

agreement with the literature value.[23]

$$TCNQ + e^- \rightleftharpoons [TCNQ]^{\bullet -} \quad (1)$$

$$[TCNQ]^{\bullet -} + e^- \rightleftharpoons [TCNQ]^{2-} \quad (2)$$

Addition of $Co^{2+}_{(MeCN)}$ ions to give either a 1:1 or 1:2 $Co^{2+}_{(MeCN)}$:TCNQ concentration ratio, led to the appearance of a sharp reduction process (labeled as process I_{red} in Figure 1) at more negative potentials ($E_p^{red} = -0.05$ V) than the $[TCNQ]^{0/\bullet -}$ process (0.170 V), but prior to the onset of the $[TCNQ]^{\bullet -/2-}$ reduction process (−0.380 V). On reversing the scan direction at −0.15 V, an oxidation counterpart (labeled as I_{ox} in Figure 1) is detected at $E_p^{ox} \approx 0.23$ V, which has the symmetrical shape associated with the stripping of a surface-confined material.[24] Scanning the potential to more negative values (−0.75 V) for the 1:2 $Co^{2+}_{(MeCN)}$:TCNQ ratio enabled the detection of the $[TCNQ]^{\bullet -/2-}$ process, as shown in Figure 1, but with a diminished peak current relative to that found in the absence of $Co^{2+}_{(MeCN)}$ ions. This $[TCNQ]^{\bullet -/2-}$ process completely vanishes when the $Co^{2+}_{(MeCN)}$ concentration is equal to or higher than 1.2 equiv.

Since the Co^{2+}/Co^0 reduction process in acetonitrile (0.1 M [NBu_4][ClO_4]) occurs at very negative potentials ($E_p^{red} \approx -1.0$ V), it is unlikely that process I_{red} (at −0.05 V) results from reduction of cobalt(II) to cobalt metal and process I_{ox} from its subsequent stripping. Since the generation of $[TCNQ]^{\bullet -}$ occurs at 0.17 V, prior to process I_{red}, $[TCNQ]^{\bullet -}$ is likely to be the species responsible for the electrocrystallization of an insoluble cobalt−TCNQ material and not the dianionic species, $[TCNQ]^{2-}$. On the basis of this scenario, the sharp reduction (I_{red}) and oxidation (I_{ox}) processes are attributed to deposition and stripping of $Co[TCNQ]_2$-based material from the electrode surface, as illustrated by overall eqs 3 and 4, respectively.

$$2TCNQ_{(MeCN)} + Co^{2+}_{(MeCN)} + 2e^- \xrightarrow{\text{deposition}} Co[TCNQ]_{2(s)} \quad (3)$$

$$Co[TCNQ]_{2(s)} \xrightarrow{\text{stripping}} 2TCNQ + Co^{2+}_{(MeCN)} + 2e^- \quad (4)$$

Voltammetric behavior analogous to that described above at a GC electrode is observed at metallic (platinum and gold) or

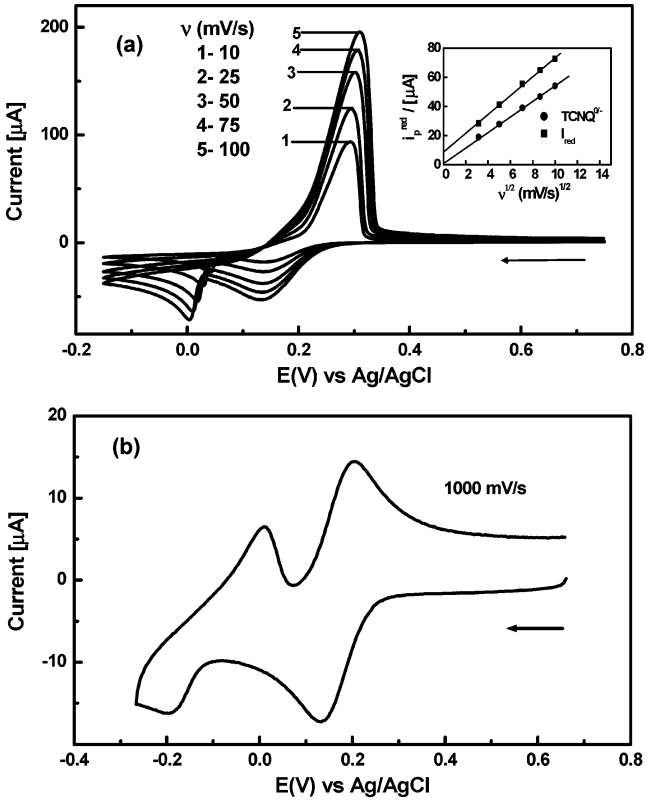

Figure 2. (a) Cyclic voltammograms obtained at a 3 mm GC electrode in acetonitrile (0.1 [NBu_4][ClO_4]) for 1.0 mM $Co(ClO_4)_2 \cdot 6H_2O$ and 2.0 mM TCNQ (1:2) with scan rates of 10−100 mV s^{-1}. The inset shows the dependence of i_p^{red} on the square root of the scan rate for $[TCNQ]^{0/\bullet -}$ and I_{red}. (b) Cyclic voltammogram obtained at lower concentrations, 0.1 mM $Co(ClO_4)_2$ and 0.2 mM TCNQ, and a higher scan rate of 1000 mV s^{-1}.

semiconducting (indium tin oxide) electrodes, thereby implying that the identity of the electrode material does not play an important role in the electrocrystallization process, as also found in the CuTCNQ case.[10c] In contrast, a marked dependence on scan rate, concentration of $Co^{2+}_{(MeCN)}$ ions, and the $Co^{2+}_{(MeCN)}$:TCNQ stoichiometric ratios is observed, particularly for processes I_{red} and I_{ox}. Cyclic voltammograms for 1.0 mM $Co^{2+}_{(MeCN)}$ and 2.0 mM TCNQ solution (Figure 2a) as a function of scan rate demonstrate that, despite the obvious independence of the $[TCNQ]^{0/\bullet -}$ process on scan rate (E_p^{red} almost constant), the reduction peak potential, E_p^{red}, associated with process I_{red} shifts to more negative values by ca. 40 mV when the scan rate is increased from 10 to 100 mV s^{-1}. Moreover, the reduction peak currents, i_p^{red}, of the two processes ($[TCNQ]^{0/\bullet -}$ and I_{red}) are proportional to the square root of scan rate, $\nu^{1/2}$ (inset in Figure 2a). Analysis of these data implies that, while reduction of TCNQ is controlled by diffusion (plot passes through the origin), reduction wave I_{red} involves a nucleation process (positive intercept on the current axis).[25] Interestingly, at lower $Co^{2+}_{(MeCN)}$ concentrations (≤0.1 mM) and at faster scan rates (≥1000 mV s^{-1}), the oxidative stripping process I_{ox} becomes well resolved from that for oxidation of $[TCNQ]^{\bullet -}$. Under these particular conditions, both the $[TCNQ]^{0/\bullet -}$ and I_{red} reduction waves have diffusion-controlled shapes (see Figure 2b). It would seem that a combination of fast scan rates (short reaction times) and low $Co^{2+}_{(MeCN)}$ concentrations provides a condition where the extent of electrocrystallization is limited, and so the reductive voltammetry is, in large part, associated with formation of a

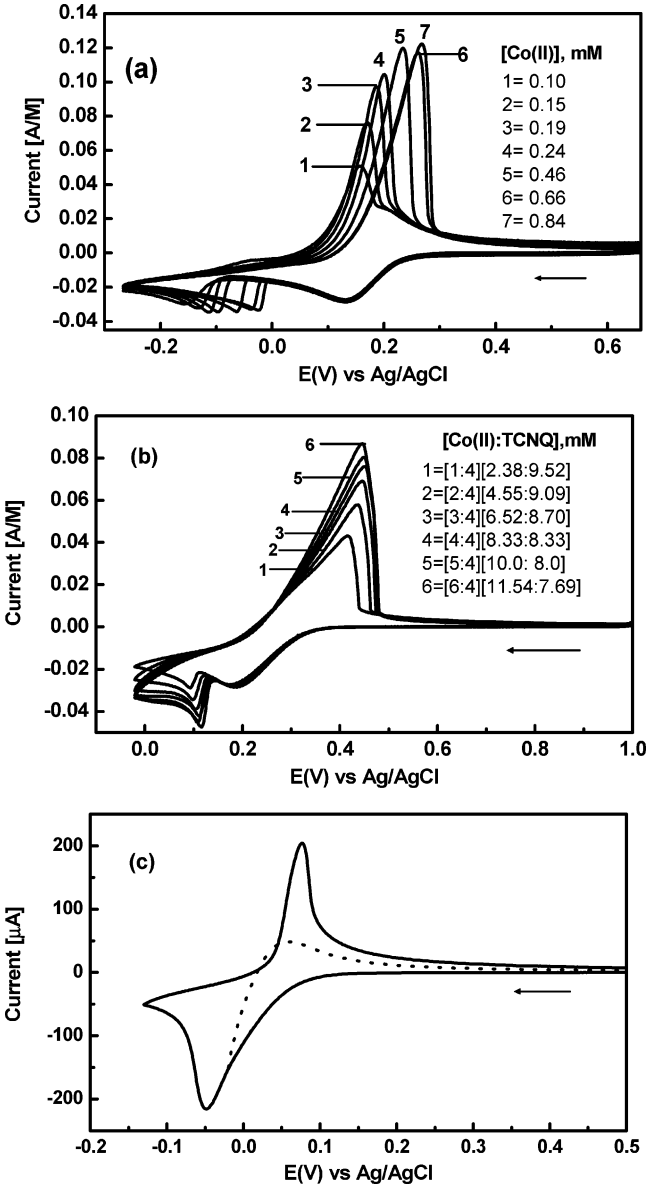

Figure 3. (a) Concentration-normalized cyclic voltammograms obtained at a scan rate of 100 mV s^{-1} in acetonitrile (0.1 [NBu$_4$][ClO$_4$]) with a 3 mm GC electrode for the reduction of TCNQ in the presence of different $Co(NO_3)_2$·6H$_2$O concentrations at a 1:2 ($Co^{2+}_{(MeCN)}$: TCNQ) ratio and in the low TCNQ concentration regime. (b) Concentration-normalized cyclic voltammograms obtained under the same conditions as (a), but at different $Co^{2+}_{(MeCN)}$:TCNQ ratios (1:4 to 6:4) and higher concentration regimes, as indicated. (c) Cyclic voltammograms obtained under the same conditions as (a), but for a mixture of 10 mM TCNQ and 5 mM $Co(ClO_4)_2$·6H$_2$O at a 1:2 ratio.

transiently soluble Co(II)−TCNQ complex. Thus, voltammetric behavior at low TCNQ concentrations (0.20−1.68 mM) was examined in the presence of $Co(NO_3)_2$ salt at a 1:2 stoichiometric ratio of $Co^{2+}_{(MeCN)}$ to TCNQ (Figure 3a). Essentially identical diffusion-controlled $[TCNQ]^{0/\bullet-}$ reduction processes were seen under these conditions if the potential was switched prior to the onset of process I_{red}. In contrast, the reduction

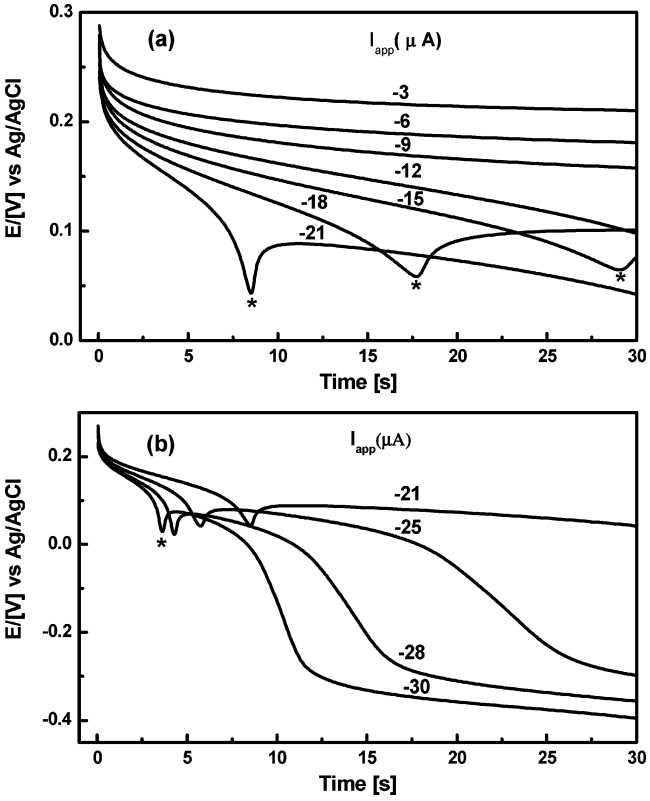

Figure 4. Potential−time galvanostatic plots obtained over a 30 s period with a 3 mm diameter GC electrode in acetonitrile (0.1 M [NBu$_4$][ClO$_4$]) when 2.20 mM TCNQ is reduced in the presence of 1.10 mM $Co(ClO_4)_2$·6H$_2$O by application of the designated constant cathodic currents: (a) from −3 to −21 μA and (b) from −21 to −30 μA.

process I_{red} exhibited a marked dependence on the $Co^{2+}_{(MeCN)}$ concentration. Thus, the peak potentials for both the reduction (E_p^{red}) and oxidation (E_p^{ox}) components associated with processes I_{red} and I_{ox} shift to more positive values by 118 and 100 mV, respectively, as the $Co^{2+}_{(MeCN)}$ concentration increases from 0.10 to 0.84 mM. The net effect is that the separation of the two reduction steps, $\Delta E_p^{red} = [E_p^{red}([TCNQ]^{0/\bullet-}) - E_p^{red}(I_{red})]$, decreases from 285 mV to about 167 mV, which implies that deposition of Co[TCNQ]$_2$-based material is more kinetically and/or thermodynamically favored at higher $Co^{2+}_{(MeCN)}$ concentrations. Furthermore, despite the almost constant peak height of i_p^{red}, the peak height (i_p^{ox}) for the coupled stripping process, I_{ox}, gradually increases with an increase in $Co^{2+}_{(MeCN)}$ concentration. Thus, process I_{ox} was further probed by holding the potential at −0.15 V vs Ag/AgCl for 1 s before scanning the potential in the positive direction from −0.15 to 0.75 V at a scan rate of 100 mV s^{-1}. Voltammograms obtained in this manner (Figure S1, Supporting Information) show that E_p^{ox} and i_p^{ox} are both largely influenced by the $Co^{2+}_{(MeCN)}$ concentration in this low TCNQ concentration regime, thereby indicating that the amount of deposited solid is significantly enhanced by increasing the $Co^{2+}_{(MeCN)}$ concentration.

Figure 3b provides concentration-normalized cyclic voltammograms at a scan rate of 100 mV s^{-1} for the high TCNQ concentration regime (∼9.5 to 7.7 mM) and with $Co^{2+}_{(MeCN)}$:TCNQ ratios covering the range of 1:4 to 6:4. As found in the low TCNQ concentration regime, relevant to Figure 3a, the $[TCNQ]^{0/\bullet-}$ reduction process remains diffusion-controlled and almost independent of the $Co^{2+}_{(MeCN)}$:TCNQ ratio. In contrast,

(23) Lehmann, M. W.; Evans, D. H. *J. Phys. Chem. B* **1998**, *102*, 9928. (b) Macías-Ruvalcaba, N. A.; Evans, D. H. *J. Phys. Chem. B* **2006**, *110*, 5155.
(24) (a) Bard, A. J.; Faulkner, L. R. *Electrochemical Methods*, 2nd ed.; Wiley: New York, 2001. (b) Murray, R. W., Ed. *Molecular Designing of Electrode Surfaces*; John Wiley and Sons: New York, 1992.
(25) Gunawardena, G.; Hills, G.; Montenegro, I. *J. Electroanal. Chem.* **1985**, *184*, 371.

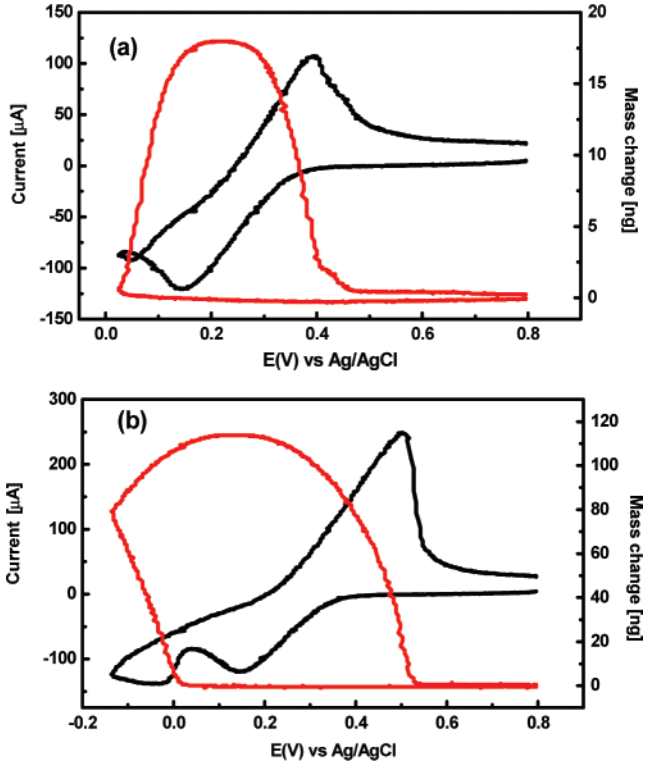

Figure 5. EQCM data (current, black; mass, red) obtained under conditions of cyclic voltammetry at scan rate of 100 mV s^{-1} using a 5 mm diameter Au electrode for 1.0 mM $Co(NO_3)_2 \cdot 6H_2O$ and 2.0 mM TCNQ (1:2 ratio) in acetonitrile (0.1 M $[NBu_4][ClO_4]$) at switching potentials (E_s) of (a) 0.03 and (b) −0.15 V.

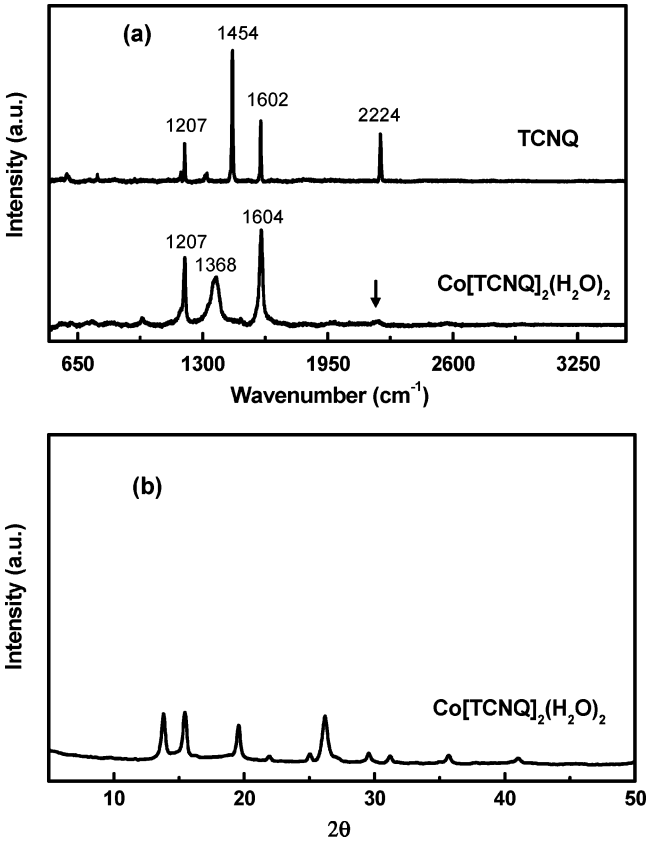

Figure 6. (a) Raman spectra of solid TCNQ crystals and electrocrystallized $Co[TCNQ]_2(H_2O)_2$. (b) X-ray powder diffraction pattern of a bulk sample of electrocrystallized $Co[TCNQ]_2(H_2O)_2$.

both of the peak potentials and peak currents for processes I_{red} and I_{ox} exhibited a marked dependence on this ratio. In particular, on increasing the ratio from 1:4 (2.38:9.52 mM) to 6:4 (11.54:7.69 mM), both peak currents (i_p^{red}, i_p^{ox}) increase in height while the peak potentials (E_p^{red}, E_p^{ox}) shift slightly to more positive potential. In fact, since process I_{red} (for all ratios) has drastically shifted to more positive potentials in this high TCNQ concentration regime, the separation of the two reduction processes, ΔE_p^{red}, is now quite small (67 mV). Moreover, it is possible under the conditions of Figure 3c to have process I_{red} merged with the $[TCNQ]^{0/\bullet -}$ process, to give a shape that is typical of a surface-confined process.[24] Taken together, these concentration results demonstrate that process I_{red} and its oxidation counterpart I_{ox} are strongly dependent on both the $Co^{2+}_{(MeCN)}$ concentration and the $Co^{2+}_{(MeCN)}$:TCNQ ratio, and that $Co^{2+}_{(MeCN)}$ ions play a crucial role in manipulating the thermodynamics and kinetics of precipitation of the corresponding $Co[TCNQ]_2$-based material.

B. Galvanostatic Reduction of TCNQ in the Presence of $Co^{2+}_{(MeCN)}$ Ions. Galvanostatic experiments at constant cathodic current readily allow assignment of the time-dependent potential changes that take place during the course of TCNQ reduction and electrocrystallization of $Co[TCNQ]_2$-based material. The $E-t$ curves generated as a result of applying cathodic current to a GC electrode in the range of −3 to −30 μA are displayed in Figure 4. Reductive electrolysis at low current (−3 to −12 μA, Figure 4a) produces the potentials expected when TCNQ is reduced by one electron to its monoanionic radical, $[TCNQ]^{\bullet -}$. Use of a larger cathodic current of −15 μA gives rise to a "potential spike" (labeled with an asterisk in Figure 4a) at 0.065 V after about 29 s. This spike becomes sharper, shifts to more negative potentials, and is also evident at earlier times at higher cathodic currents (Figure 4b). The constant potential value of 0.03 V obtained after ~3.5 s of applying a cathodic current of −30 μA is similar to that for process I_{red} under potentiostatic conditions. The final constant potential region achieved at −0.3 V for a constant current of −30 μA corresponds to the value expected for the onset of the $[TCNQ]^{\bullet -/2-}$ reduction process.[10e] The potential spike produced galvanostatically and the reduction process I_{red} "current spike" detected potentiostatically are both believed to have the same origin and to be associated with electrodeposition of $Co[TCNQ]_2$-based material.

C. EQCM Detection of Potential-Dependent Electrocrystallization Processes. Voltammetric and galvanostatic data for reduction of TCNQ in the presence of $Co^{2+}_{(MeCN)}$ ions suggest that a $Co[TCNQ]_2$-based material is deposited onto the electrode surface during the course of process I_{red} and then stripped off via process I_{ox}. EQCM experiments should allow the mass changes to be detected on the electrode surface, if this hypothesis is valid.

EQCM data obtained at a scan rate of 100 mV s^{-1} for reduction of 2.0 mM TCNQ in the presence of 1.0 mM $Co^{2+}_{(MeCN)}$ ions at a 5 mm diameter gold electrode are shown in Figure 5. The cyclic voltammetric component of the experiment is similar to that found with 1−3 mm diameter GC, Pt, or Au macrodisk electrodes, except that use of a larger Au electrode results in an enhanced ohmic (iR_u) drop effect. However, and somewhat unexpectedly, scanning the potential negatively from an initial value (E_i) of 0.8 V to switching potentials (E_s) of 0.065 V (Figure S2) or 0.03 V (Figure 5a), but prior to the onset of

process I_{red}, produces a significant mass increase near the switching potential (Sauerbrey equation assumed to be valid). The observation that only a minimal increase in mass is detected at the potential where TCNQ reduction begins implies that a delay period occurs prior to the rapid growth stage of this newly detected deposition process. On reversing the scan direction, the mass continues to increase sharply due to continued deposition of a solid material at the electrode surface, until the maximum mass value is obtained just prior to the potential where $[TCNQ]^{\bullet -}$ is oxidized back to neutral TCNQ ($[TCNQ]^{\bullet -}$ no longer generated). At more positive potentials, the mass decreases rapidly in the potential region where voltammetric data suggest that oxidation of the electrodeposited Co[TCNQ]$_2$-based material is expected to regenerate soluble TCNQ and $Co^{2+}_{(MeCN)}$ ions. However, the mass does not return completely to the initial or baseline value upon completion of each potential cycle, implying that not all deposited solid is removed from the surface when Co[TCNQ]$_2$-based material is electrocrystallized at potentials prior to the onset of process I_{red} (vide infra).

When E_s is made more negative than process I_{red}, voltammograms now encompass the potential region where, according to voltammetric data, deposition of a Co[TCNQ]$_2$-based material should occur via the two reduction processes ($[TCNQ]^{0/\bullet -}$ and I_{red}). Indeed, a far greater rate increase in mass is detected at the onset of process I_{red} than prior to reaching this potential. This rapid increase in mass continues until the switching potential of -0.15 V is reached (Figure 5b), and also after the potential scan direction is reversed, until a maximum value is obtained at about 0.15 V. Upon approaching the stripping region associated with process I_{ox} (0.16$-$0.54 V), a significant decrease in mass is observed and almost a complete loss of mass is achieved by the time the potential is returned to its initial value. Furthermore, when the EQCM experiment, under the conditions of Figure 5b, is repeated over 20 cycles of the potential, the mass always returns back to the baseline value at the end of each cycle. This EQCM finding is consistent with the conclusion based on repetitive potential cycling voltammetric experiments performed at a range of electrodes (see Figure S3 at a GC electrode), where identical cyclic voltammetric responses were obtained for each cycle, which is expected if the stripping process I_{ox} successfully removes all of the electrocrystallized solid, formed during the deposition step, when the potential is scanned in the positive direction. Moreover, a linear dependence of mass gain on the switching potential (E_s) is obtained at values more negative than process I_{red} (Figure S4), as expected for a process governed by nucleation.[26] All the EQCM results suggest that the reaction mechanism for deposition of Co[TCNQ]$_2$-based solid is potential-dependent and most likely follows a different pathway at more negative potential regimes than is the case when solid is deposited prior to the onset of process I_{red}.

II. Characterization of the Electrocrystallized Co[TCNQ]$_2$-Based Solid. The main features of the electrocrystallization process can be certainly described by eqs 5 and 6.

$$TCNQ_{(MeCN)} + e^- \rightleftharpoons [TCNQ]^{\bullet -}_{(MeCN)} \quad (5)$$

$$2[TCNQ]^{\bullet -}_{(MeCN)} + Co^{2+}_{(MeCN)} \rightarrow Co[TCNQ]_{2(s)} \quad (6)$$

(26) Ward, M. D. *J. Electroanal. Chem.* **1989**, *273*, 79.

However, since several forms of Co[TCNQ]$_2$-based materials[27] are known to exist, it is necessary to identify the composition and phase formed under electrochemical conditions. Reductive bulk electrolysis (electrocrystallization) from an acetonitrile (0.1 M $[NBu_4][ClO_4]$) solution containing 10 mM TCNQ and 5 mM $Co(ClO_4)_2$ at $E_{app} = -0.1$ V (more negative than process I_{red}) results in a rapid solution color change from yellow to deep green with concomitant deposition of dark blue solid material at large platinum foil or basket electrode surfaces. Upon completion of the electrocrystallization process (1.05 F/equiv, several hours), the majority of the solid crystalline material formed was adhered strongly to the surface of the working electrode as a compact film. After removal from the electrode surface and washing several times with acetonitrile to remove supporting electrolyte, the dried solid was then examined by a range of spectroscopic and microscopic techniques. Solid obtained by reductive electrolysis at shorter times (10 min to 30 s) and at potentials prior to and more negative than process I_{red} also was collected from a range of electrode surfaces and then subjected to the same methods of characterization.

A. IR Spectroscopy. IR spectra obtained from all solids electrodeposited for extended periods at potentials either before or after process I_{red} onto GC, ITO electrodes, or larger surface area Pt foil or basket electrodes from 1:1 or 1:2 $Co^{2+}_{(MeCN)}$:TCNQ ratios (with or without removal of excess $[NBu_4][ClO_4]$ electrolyte) exhibited IR bands that are characteristic of Co[TCNQ]$_2$(H$_2$O)$_2$.[13b,18] Thus, three intense IR bands[28] were found in the ν(C≡N) region at 2219, 2203, and 2178 cm^{-1}, which are as expected for the $[TCNQ]^{\bullet -}$ anion radical rather than for $[TCNQ]^{2-}$ dianion or neutral TCNQ.[29] The electrocrystallized solid also exhibited a strong IR band at 1505 cm^{-1}, together with a sharp δ(C−H) IR stretch at 824 cm^{-1}, consistent with the presence of the $[TCNQ]^{\bullet -}$ anion radical and not the $[TCNQ-TCNQ]^{2-}$ σ-dimer[13b] or neutral TCNQ (864 cm^{-1}). Finally, the absence of MeCN stretches at (∼2314 and 2286 cm^{-1})[15] and the presence of two broad absorption IR bands at 3425 and 3343 cm^{-1}, along with a weak band at ca. 1642 cm^{-1} (Figure S5), support the presence of water molecules, either as coordinated or adsorbed water, and not MeCN. The IR data strongly suggest that the electrocrystallized product is the hydrated Co[TCNQ]$_2$(H$_2$O)$_2$ phase. Importantly, despite detection of two different pathways for electrocrystallization, apparently the same Co[TCNQ]$_2$(H$_2$O)$_2$ solid is formed in either case. If short electrolysis periods are used, sometimes only two IR bands are detected in the ν(C≡N) region.[28]

B. Raman Spectroscopy. Figure 6a provides a comparison of the Raman spectra of electrocrystallized Co[TCNQ]$_2$-based material and neutral TCNQ solids. The four most intense Raman vibrations (1207, 1454, 1602, and 2224 cm^{-1}) present in the TCNQ spectrum include one at 1454 cm^{-1}, which corresponds to the C═C ring stretching mode of TCNQ. This band is shifted by 86 cm^{-1} as a result of reduction of TCNQ into $[TCNQ]^{\bullet -}$

(27) These include, in addition to the solvent-free Co[TCNQ]$_2$, the acetonitrile solvated phase Co[TCNQ](MeCN)$_2$ and the hydrated phases such as Co[TCNQ]$_2$(H$_2$O)$_2$ and Co[TCNQ]$_2$(H$_2$O)$_3$. Coordinated water in these hydrated phases may result from either adventitious water in acetonitrile or the hydrated Co(II) salts.

(28) Thin films obtained after short electrolysis times (30−240 s) show only two strong IR bands in the ν(C≡N) region at 2200 and 2134 cm^{-1}, consistent with materials chemically synthesized via a $[Co(MeCN)_6][SbF_6]_2$ precursor.[15] This is probably associated with generation of non-hydrated Co[TCNQ]$_2$ under these conditions.

(29) Khatkale, K. S.; Devlin, J. P. *J. Chem. Phys.* **1979**, *70*, 1851.

and formation of a Co[TCNQ]$_2$-based material. This shift is consistent with that obtained from an authentic sample of the hydrated Co[TCNQ]$_2$(H$_2$O)$_2$ complex[13b,18] and those reported for other MTCNQ compounds (M = Cu, Ag, or alkali metals),[29,30] thereby indicating the presence of [TCNQ]$^{\bullet-}$ in the electrocrystallized material and formation of the hydrated phase. Furthermore, the shift of 12 cm^{-1} in the 2224 cm^{-1} band, along with a reduction of its intensity,[30c] also provides a spectroscopic fingerprint for the formation of Co[TCNQ]$_2$(H$_2$O)$_2$.

C. Elemental and Thermogravimetric Analyses. Elemental analysis[31] results of isolated electrocrystallized samples also are consistent with the empirical formula of Co[TCNQ]$_2$(H$_2$O)$_2$. The more definitive TGA data (Figure S6) confirm the presence of two water molecules (two dehydration steps), corresponding to loss of ~7% of the mass at temperatures below 230 °C. At temperatures above 230 °C, a large change in mass occurs, indicative of decomposition via loss of TCNQ, as previously observed with chemically synthesized Co[TCNQ]$_2$(H$_2$O)$_2$.[13b]

D. Powder X-ray Diffraction. Conventional X-ray diffraction (XRD) powder patterns obtained from bulk electrocrystallized (several hours) Co[TCNQ]$_2$-based materials contain diffraction peaks at 2θ values of 13.83°, 15.47°, 19.57°, 21.94°, 25.05°, 26.21°, 29.57°, 31.20°, 35.70°, and 41.03° (Figure 6b). These closely match values obtained for Co[TCNQ]$_2$(H$_2$O)$_2$ generated via aqueous solid−solid phase electrochemical transformation of TCNQ in the presence of Co$^{2+}_{(aq)}$[18] and for chemically synthesized Co[TCNQ]$_2$(H$_2$O)$_2$.[13b] Thus, these XRD data confirm that the long-term electrocrystallized product is Co[TCNQ]$_2$(H$_2$O)$_2$ and not Co[TCNQ](MeCN)$_2$[17a] or the non-hydrated Co[TCNQ]$_2$ phase,[14] and that isolated solids samples are crystalline rather than amorphous in nature.

Ex situ synchrotron radiation grazing X-ray diffraction (SR-GIXRD) measurements performed at a wavelength of 1.0 Å with thin films of Co[TCNQ]$_2$-based materials deposited on ITO surfaces with short electrolysis times (2−4 min) showed preferred orientations, as evidenced by detection of only a small number of intense diffraction peaks at 2θ values of ca. 5.25°, 10.50°, and 15.30°. These diffraction values are different from those obtained for the hydrated Co[TCNQ]$_2$(H$_2$O)$_2$ phase using long-scale electrolysis times and a conventional laboratory-based diffractometer (at λ = 1.5418 Å they would have appeared at 8.30°, 16.62°, and 24.20°), but they closely match with the literature diffraction data for the non-hydrated Co[TCNQ]$_2$ phase.[14] The values are also close to the experimentally determined 2θ values for the [NBu$_4$][ClO$_4$] supporting electrolyte (8.40°, 16.86°, and 24.26°) obtained from conventional XRD measurement. However, given the high intensity for the major diffraction peak at a 2θ value of 5.25° (e.g., 400 000 counts at an angle of incidence of 0.4°) and the fact that the electrodeposited films were washed several times with pure acetonitrile to remove [NBu$_4$][ClO$_4$], the observed diffraction peaks are attributed to the non-hydrated Co[TCNQ]$_2$ phase. This is consistent with IR evidence obtained at short electrolysis times.[28]

It would have been anticipated that a mixture of anhydrous Co[TCNQ]$_2$ and hydrated Co[TCNQ]$_2$(H$_2$O)$_2$ might have been

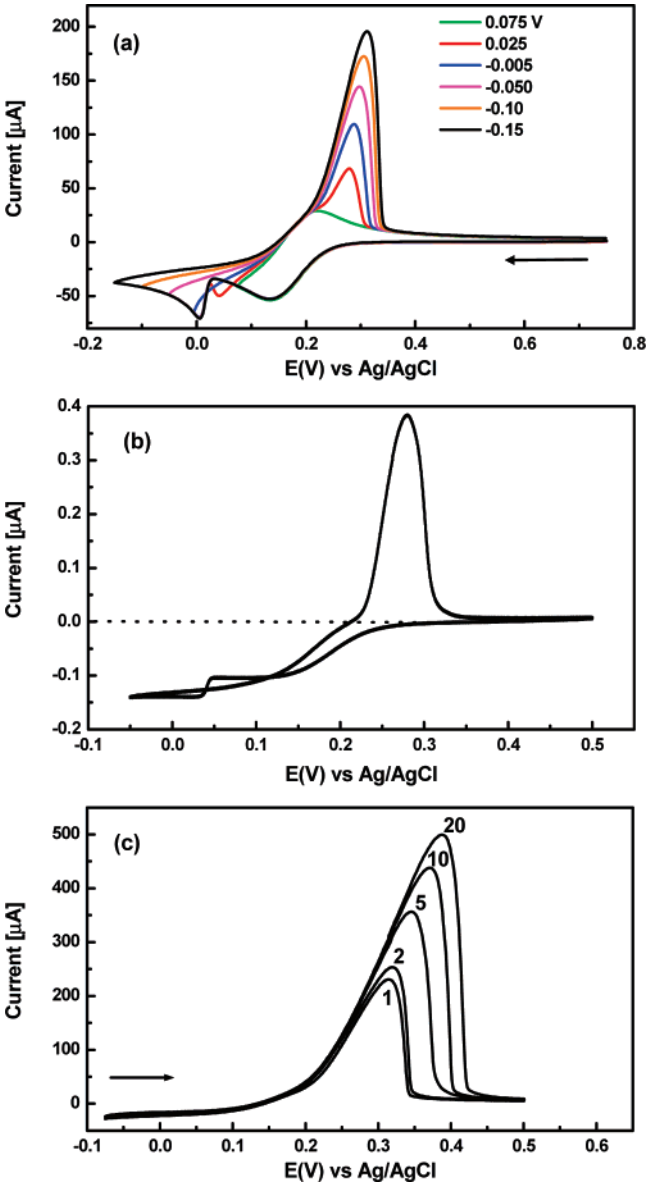

Figure 7. Voltammograms obtained with a 3 mm diameter GC macrodisk electrode from a mixture of 1.10 mM Co(ClO$_4$)$_2$·6H$_2$O and 2.20 mM TCNQ in acetonitrile (0.1 M [NBu$_4$][ClO$_4$]) when the potential (a) is switched to the designated potential at a scan rate of 20 mV s^{-1}. (b) Conditions as for (a), but with a 125 μm diameter Au microdisk electrode at a scan rate of 100 mV s^{-1}. (c) Conditions as for (a), but when the potential is held at −0.075 V for the designated time intervals and then scanned in the positive potential direction at a scan rate of 100 mV s^{-1}.

detected in the SR-GIXRD measurments. Detection of the Co[TCNQ]$_2$ phase is interesting in the sense that it implies it is formed either in the initial stage of electrolysis, prior to its eventual hydration to Co(TCNQ)$_2$(H$_2$O)$_2$, as proposed in reaction Schemes 1 and 2 (vide infra), or it results from removal of water molecules (dehydration) from the Co(TCNQ)$_2$(H$_2$O)$_2$ phase under dehumidified experimental conditions, which would, indeed, account for the poor crystallinity of the films. It is therefore significant to note that the SR-GIXRD patterns obtained for the electrodeposited thin films at an angle of incidence of 0.1° (this detected the electrodeposited film and none of the underlying ITO substrate) revealed high background counts at low 2θ values, which provided evidence to support

(30) (a) Kamitsos, E. I.; Risen, W. M., Jr. *J. Chem. Phys.* **1983**, *79*, 5808. (b) Kamitsos, E. I.; Risen, W. M., Jr. *Mol. Cryst. Liq. Cryst.* **1986**, *134*, 31. (c) Ye, C.; Cao, G.; Fang, F.; Xu, H.; Xing, X.; Sun, D.; Chen, G. *Micron* **2005**, *36*, 461.

(31) Elemental analysis was performed at Campbell Microanalytical Laboratory. Calcd for C$_{24}$H$_{12}$CoN$_8$O$_2$: C, 57.27; H, 2.40; N, 22.26. Found: C, 57.93; H, 2.53; N, 21.47.

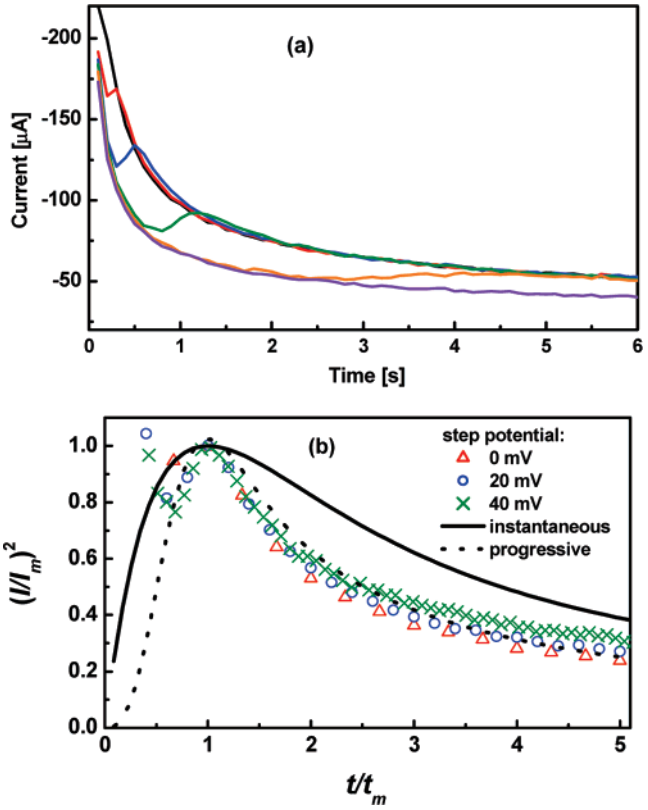

Figure 8. (a) Chronoamperometric ($i-t$) transients obtained with a 3 mm GC electrode for a mixture of $Co(ClO_4)_2 \cdot 6H_2O$ (1.25 mM) and TCNQ (2.50 mM) in acetonitrile (0.1 M $[NBu_4][ClO_4]$) when the potential is stepped from an initial value (0.75 V) to more negative potentials (0.08 to −0.02 V with 20 mV increments). (b) Comparison of experimental plot of $(i/i_m)^2$ vs t/t_m obtained from chronoamperometric experimental results and theoretical nondimensional plots derived from the instantaneous (—) and progressive nucleation (---) models using the equation $(i/i_m)^2 = [1.2254/(t/t_m)]\{1 - \exp[-2.3367(t/t_m)^2]\}^2$ and $(i/i_m)^2 = [1.9542(t/t_m)]\{1 - \exp[-1.2564(t/t_m)]\}$, respectively.[36b,c]

the formation of poorly crystalline $Co(TCNQ)_2(H_2O)_2$ under these dehumidified, short electrolysis time conditions. Finally, a depth profile of the electrodeposited $Co[TCNQ]_2$-based material on ITO, as obtained by varying the angle of incidence from 0.1° to 4°, revealed that the thickness of the film is between 1.8 and 7.0 μm.

E. Solubility Measurements. The solubility of electrocrystallized $Co[TCNQ]_2(H_2O)_2$ in acetonitrile was determined by monitoring the concentration of liberated $[TCNQ]^{\bullet-}$ over a period of one week, using UV/vis spectrophotometry in the absence of electrolyte and voltammetry at a 125 μm diameter gold microelectrode in the presence of electrolyte. In the absence of electrolyte, the solubility was found to be 0.066 ± 0.005 mM. The presence of 0.1 M $[NBu_4][ClO_4]$ increased the solubility to 0.234 ± 0.015 mM, which, as in the case of the CuTCNQ analogue,[10c] is most likely due to introduction of ion pairing with electrolyte ions. The calculated solubility product (K_{sp}) of $Co[TCNQ]_2(H_2O)_2$ is 2.84×10^{-13} M^3 without electrolyte and 1.28×10^{-11} M^3 with electrolyte. Thus, in order for electrocrystallization of $Co[TCNQ]_2(H_2O)_2$ to occur in acetonitrile/0.1 M $[NBu_4][ClO_4]$, from a thermodynamic perspective, the ion product, $[Co^{2+}][TCNQ^{\bullet-}]^2$, needs to exceed the solubility product[26] (1.28×10^{-11} M^3). This requirement is met for all experiments undertaken in this study.

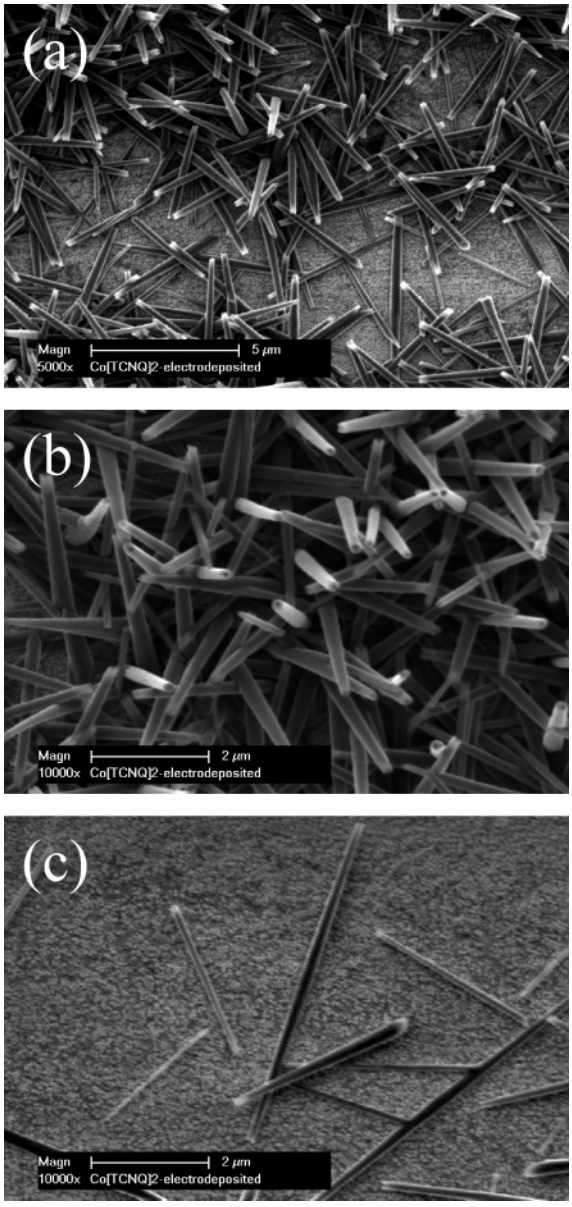

Figure 9. SEM images obtained at different magnifications after reductive electrolysis at an ITO electrode from a mixture of 1.0 mM $Co(ClO_4)_2 \cdot 6H_2O$ and 2.0 mM TCNQ in acetonitrile (0.1 M $[NBu_4][ClO_4]$) at $E_{app} = 0.05$ V (before process I_{red}) for 180 s.

III. Evidence for a Progressive Nucleation−Growth Mechanism. The nucleation−growth mechanism of a deposited solid affects both the size and properties of the resulting crystals.[32] Despite extensive recent research efforts devoted to studying the deposition and growth mechanism of metals, relatively few new insights have been gained in the area of electrocrystallization of metal−organic solids.[33] This is probably due to the greater complexity of processes where deposits are formed on the surface as a result of a combination of electron transfer and chemical reactions. In the present case, studies have been performed in order to probe the type of growth mechanisms involved in the electrocrystallization of $Co[TCNQ]_2(H_2O)_2$.

(32) Ward, M. D. In *Electroanalytical Chemistry*; Bard, A. J., Ed.; Dekker: New York, 1989; Vol. 16, p 181.
(33) (a) Ilangovan, G.; Zweier, J. L.; Kuppusamy, P. *J. Phys. Chem. B* **2000**, *104*, 4047. (b) Wysocka, M.; Winkler, K.; Stork, J. R.; Balch, A. L. *Chem. Mater.* **2004**, *16*, 771.

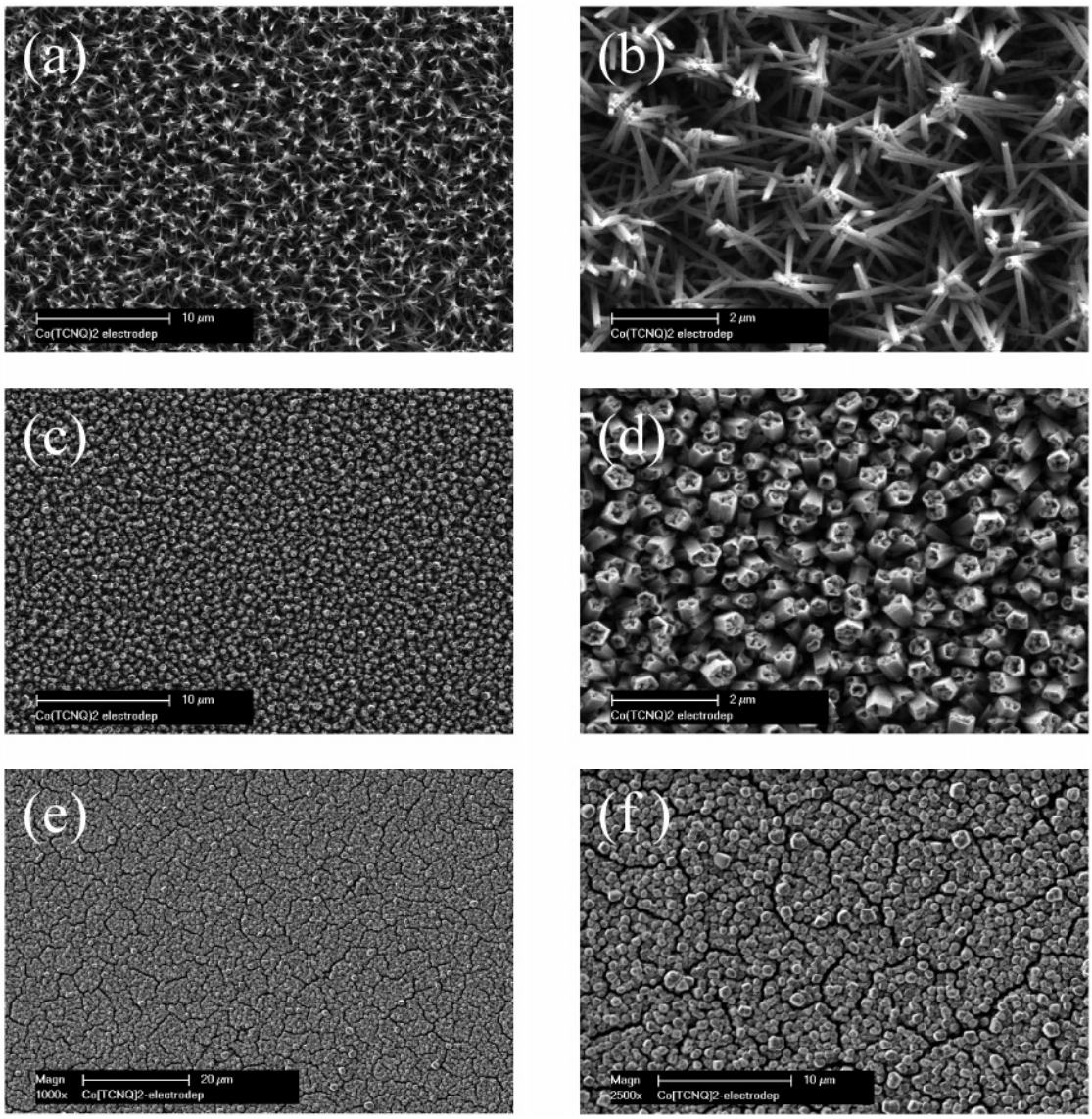

Figure 10. SEM images of electrocrystallized $Co[TCNQ]_2(H_2O)_2$ on an ITO electrode when a mixture of 2.5 mM $Co(ClO_4)_2 \cdot 6H_2O$ and 5 mM TCNQ (1:2 ratio) in acetonitrile (0.1 M [Bu4N][ClO_4]) is reduced at (a,b) 0.05 V and (c,d) −0.1 V for 180 s. (e,f) Images obtained under the same conditions as in (c,d) but at a longer electrolysis time of 300 s.

Cyclic voltammograms at a GC electrode (Figure 7a) obtained at a scan rate of 20 mV s^{-1} and with a 1:2 $Co^{2+}_{(MeCN)}$ (1.10 mM) to TCNQ (2.20 mM) concentration ratio demonstrate that stripping process I_{ox} is highly dependent upon the switching potential E_s. When E_s is 0.075 V (the diffusion-limited region), no stripping peak is detected on the reverse scan. In contrast, experiments with the same E_s value, but higher $Co^{2+}_{(MeCN)}$ and TCNQ concentrations, do exhibit stripping. This supports the EQCM finding that deposition of solid $Co[TCNQ]_2(H_2O)_2$ may occur at potentials prior to process I_{red}. Under the conditions of Figure 7a and when E_s is 0.025 V (foot of the onset of process I_{red}), current crossover occurs at 0.065 V during the course of the forward and reverse potential scans. Concomitantly, an anodic stripping process (I_{ox}) is detected. The current loop feature is generally accepted as evidence of a nucleation and growth phenomenon.[10c] As E_s is made even more negative, a marked increase in the stripping peak height (i_p^{ox}) is observed, thereby indicating that i_p^{ox} and hence deposited $Co[TCNQ]_2(H_2O)_2$ solid are highly dependent on the switching potential.

The presence of a nucleation and growth mechanism is further supported by voltammetric studies at microelectrodes. In this case, reduction of TCNQ to $[TCNQ]^{\bullet -}$ at a gold microdisk electrode occurs under near steady-state rather than transient conditions. As a consequence, when the potential is scanned in the negative direction, initially a sigmoidal-shaped $[TCNQ]^{0/\bullet -}$ process is observed (Figure 7b). At more negative potentials, process I_{red} is detected at 0.035 V, and then the current value slowly decays until the switching potential of −0.05 V is reached. On reversing the scan direction, the reductive current continues to decrease and gives rise to current crossover at 0.04 and 0.11 V, indicative of a nucleation−growth mechanism.[10c] At potentials close to the $[TCNQ]^{0/\bullet -}$ process, the reduction current rapidly decreases and becomes positive at 0.21 V when the stripping process I_{ox} commences ($E_p^{ox} = 0.28$ V). Finally, after completion of the full cycle, the current returns back to zero.

The effect of deposition time on the electrocrystallization process was investigated by monitoring the stripping responses

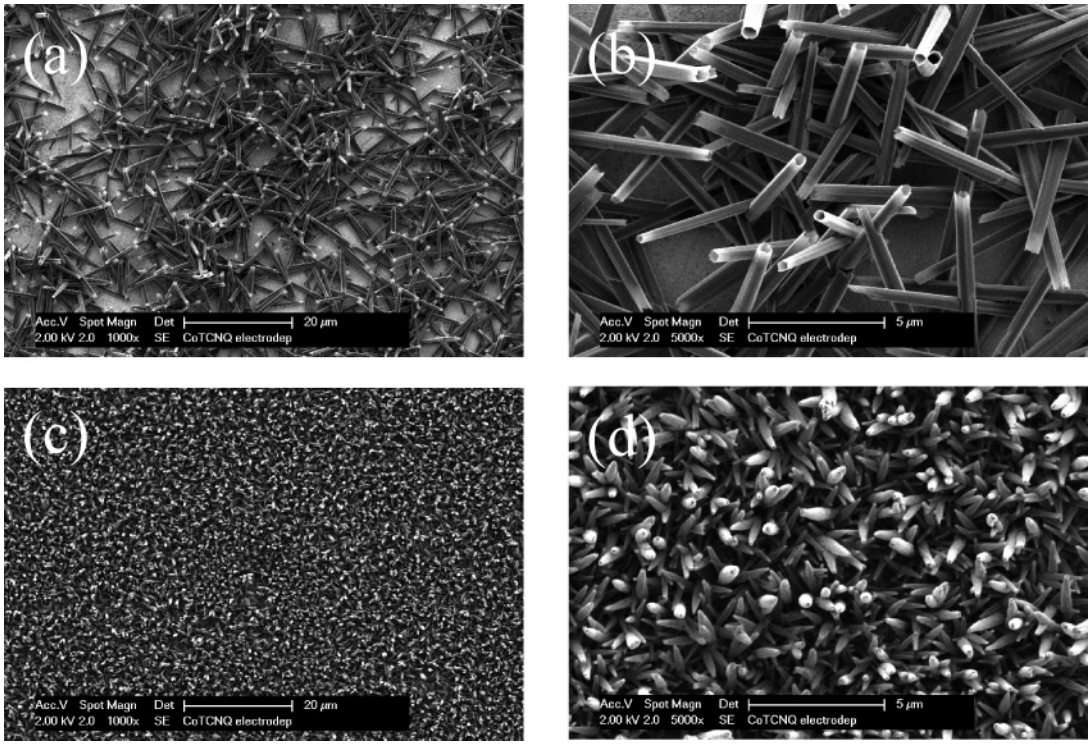

Figure 11. SEM images of electrocrystallized $Co[TCNQ]_2(H_2O)_2$ on an ITO electrode when a solution containing 2.5 mM $Co(NO_3)_2{\cdot}6H_2O$ and 5.0 mM TCNQ (1:2 ratio) in acetonitrile (0.1 M $[Bu_4N][ClO_4]$) is reduced at (a,b) 0.05 V and (c,d) −0.1 V for 180 s.

(I_{ox}) obtained under chronoamperometric-linear sweep voltammetric conditions at a 3 mm diameter glassy carbon electrode when the potential was held at −0.075 V vs Ag/AgCl for designated periods of time, followed by scanning the potential in the positive direction at a rate of 100 mV s^{-1}. As can be seen in Figure 7c, the deposition time significantly affects not only the current magnitude but also the shape of the stripping process. Both the peak height (i_p^{ox}) and peak width at half-height ($W_{1/2}^{ox}$) increase, the latter by ∼37 mV, and the peak potential (E_p^{ox}) shifts to more positive values (by ca. 75 mV) upon increasing the deposition time from 1 to 20 s. The charge associated with the stripping responses (Q_{ox}) also increases from $(2.13 \pm 0.15) \times 10^{-4}$ C (for a deposition time of 1 s) to $(6.37 \pm 0.17) \times 10^{-4}$ C at 20 s. These charge magnitudes are much larger than that expected for stripping of a monolayer of $Co[TCNQ]_2(H_2O)_2$ adsorbed on the electrode surface.[24] Thus, electrocrystallization of $Co[TCNQ]_2(H_2O)_2$ can occur onto the electrode surface at potentials when generation of $[TCNQ]^{\bullet-}$ commences, providing the kinetics of precipitation are sufficiently fast on the relevant voltammetric time scale.

Chronoamperometric data also provided access to information related to the type of nucleation and growth involved in the electrocrystallization of $Co[TCNQ]_2(H_2O)_2$. A series of potentiostatic current−time (*i*-*t*) transients obtained when the potential is stepped from 0.75 V, where no faradaic process occurs, to progressively more negative values over the range of 0.08 to −0.02 V, which corresponds to potentials encompassing the diffusion limit of $[TCNQ]^{0/\bullet-}$ reduction and process I_{red}, respectively, are presented in Figure 8a. Initially a large capacitance current is detected, which rapidly decays to the background current in less than 1 s.[33a] In contrast, the faradaic current transients, detected at longer times, rapidly increase to a maximum current value (i_m) before decreasing to the diffusion-limited value. When the potential is stepped to a very negative value relative to process I_{red}, then the well-known $t^{-1/2}$ (t = time) Cottrellian decay is detected and no current maximum is observed. Overall, the nature of the chronoamperometric curves (Figure 8a) clearly indicates that the electrocrystallization process of $Co[TCNQ]_2(H_2O)_2$ is governed by nucleation and growth kinetics.[34]

Scheme 1

$$TCNQ + e^- \underset{\text{(bulk reduction via TCNQ}^{0/-}\text{ process)}}{\rightleftharpoons} [TCNQ]^{\bullet-}$$

$$2\,[TCNQ]^{\bullet-} + Co^{2+}_{(MeCN)} \xrightarrow{\text{(nucleation/growth at defect sites)}} Co[TCNQ]_{2(s)}$$

$$Co[TCNQ]_{2(s)} + 2H_2O \longrightarrow \{Co[TCNQ]_2(H_2O)_2\}_{(s)}$$

3-D nucleation with diffusion-controlled growth represents a commonly reported model for deposition of metals, organics and metal−organic materials.[34,35] Consequently, the chronoamperometric data obtained during the electrocrystallization of $Co[TCNQ]2(H_2O)_2$ were analyzed using the methodology developed by Scharifker et. al.[36] This approach allows both instantaneous and progressive nucleation−growth mechanisms to be considered by comparison of experimental data with normalized growth laws that predict the ratio of current (i) obtained at time (t) to the maximum current (i_m) obtained at time (t_m). As can be seen in Figure 8b, the experimental plot of

(34) (a) Harrison, J. A.; Thirsk, H. R. In *Electroanalytical Chemistry*; Bard, A. J., Ed.; Dekker: New York, 1971; Vol. 5, p 67. (b) Matthijs, E.; Langerock, S.; Michailova, E.; Heerman, L. *J. Electroanal. Chem.* **2004**, *570*, 123.

(35) (a) Bosco, E.; Rangarajan, S. K. *J. Electroanal. Chem.* **1982**, *134*, 225. (b) Mirkin, M. V.; Nilov, A. P. *J. Electroanal. Chem.* **1990**, *283*, 35. (c) Heerman, L.; Tarallo, A. *J. Electroanal. Chem.* **1999**, *470*, 70. (d) Gonzalez-Garcia, J.; Gallud, F.; Iniesta, J.; Montiel, V.; Aldaz, A.; Lasia, A. *J. Electrochem. Soc.* **2000**, *147*, 2969. (e) Heerman, L.; Tarallo, A. *Electrochem. Commun.* **2000**, *2*, 85.

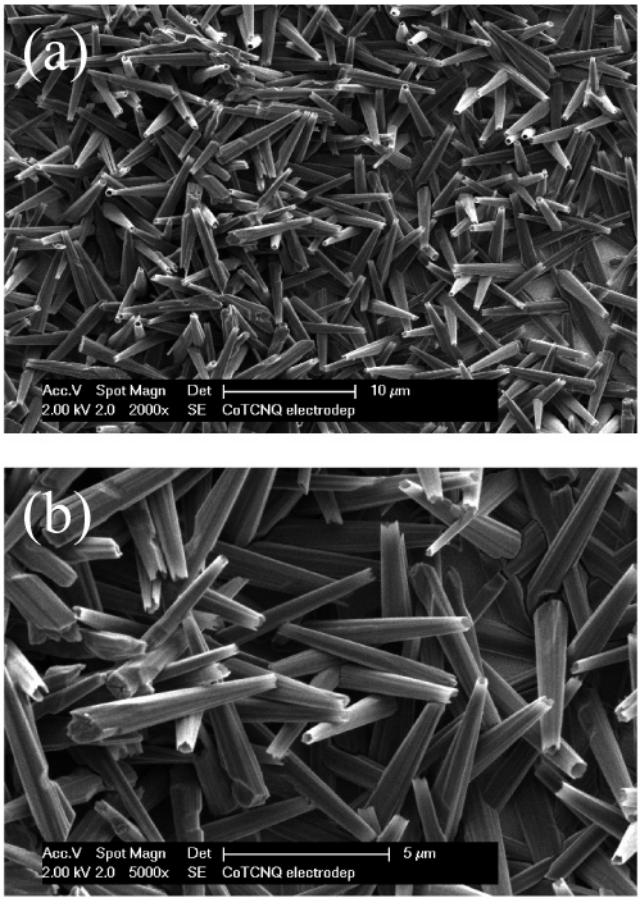

Figure 12. SEM images at (a) low and (b) high magnification of electrocrystallized $Co[TCNQ]_2(H_2O)_2$ on an ITO electrode when a mixture of 5 mM $Co(NO_3)_2{\cdot}6H_2O$ and 5 mM TCNQ (1:1 ratio) in acetonitrile (0.1 M $[Bu_4N][ClO_4]$) is reduced at 0.05 V for 180 s.

$(i/i_m)^2$ vs t/t_m for $Co[TCNQ]_2(H_2O)_2$ deposition onto a GC electrode matches well with the progressive nucleation model. This analysis therefore indicates that $Co[TCNQ]_2(H_2O)_2$ electrodeposition occurs predominantly via a progressive nucleation and growth mechanism.

IV. Morphology of $Co[TCNQ]_2(H_2O)_2$ as a Function of Potential and Concentration. SEM images of $Co[TCNQ]_2(H_2O)_2$ electrocrystallized onto an ITO electrode surface from a 1.0 mM $Co(ClO_4)_2$ and 2.0 mM TCNQ (1:2 ratio) solution in acetonitrile (0.1 M $[NBu_4][ClO_4]$) when the potential is held at 0.05 V (prior to onset of process I_{red}) for 180 s reveal the formation of well-separated, needle-shaped $Co[TCNQ]_2(H_2O)_2$ nanowires (Figure 9a). The majority of the crystals grow outward from the electrode surface, presumably from well-spaced nucleation sites. Inspection at higher magnification (Figure 9b) shows that these nanowires are hollow, at least near their tips, and have a polygonal/cone shape. Figure 9c shows an image of another region of the electrode surface, where some flat and straight nanowires, having lengths of 2−6 μm and diameters of 100−200 nm, are present.

Increasing the concentration of the $Co(ClO_4)_2$ precursor to 2.5 mM while maintaining the $Co^{2+}_{(MeCN)}$:TCNQ ratio at 1:2, under $E_{app} = 0.05$ V for 180 s, results in the deposition of more closely packed but smaller $Co[TCNQ]_2(H_2O)_2$ nanowires (Figure 10 a,b). Formation of lacunae at the tips is normally associated with growth at edges being faster than in the center of the initially formed crystals and has been previously observed in the formation of NaTCNQ[11b] and AgTCNQ.[8j] SEM images (Figure 10c,d) obtained from exactly the same solution, but when a potential more negative than process I_{red} (−0.1 V) was applied, show a remarkably different morphology, as evidenced by the presence of a closely packed, randomly oriented film of partially filled hexagonal-shaped nanorod crystals. At longer electrolysis time (5 min), the film became more densely packed, as shown in Figure 10e. Use of higher magnification (Figure 10f) reveals that these nanorods retain their hexagonal shapes but are now solid rather than hollow. EDAX analysis of the composition of electrodeposited materials confirmed the presence of cobalt along with carbon and nitrogen as required for formation of $Co[TCNQ]_2(H_2O)_2$.

Micrographs obtained from reductive electrolysis (180 s) of a mixture containing 10 mM TCNQ (close to the solubility limit of TCNQ in acetonitrile) and 5.0 mM $Co(ClO_4)_2$ show a deviation of the single-crystal growth seen for the electrocrystallized $Co[TCNQ]_2(H_2O)_2$ at lower concentrations (Figures 9 and 10a,b). Only one reduction wave is found under these conditions (see Figure 3c), and SEM images obtained at $E_{app} = 0.05$ and −0.1 V are now virtually identical and consist of disordered plate-like crystals having significant twinning and random orientation on the ITO electrode surface (Figure S7a). Moreover, SEM images of $Co[TCNQ]_2(H_2O)_2$ formed via bulk electrocrystallization at a large Pt foil electrode (Figure S7b) under the same concentration regime, but at a much longer deposition time (10 h) and after transferring the collected crystals to a carbon tape, reveal a scattered orientation of the completely filled (solid), needle-shaped crystals that are combined together into cylindrical shapes with a pinhole at their tips. Taken together, these SEM observations suggest that longer electrolysis times and/or higher concentrations are necessary to generate crystals having the morphology obtained for $Co[TCNQ]_2(H_2O)_2$ prepared via electrochemical solid−solid phase conversion of TCNQ at an aqueous interface in the presence of $Co^{2+}_{(aq)}$ ions.[18]

Different morphologies also were observed upon using $Co(NO_3)_2$ (2.50 mM) as the $Co^{2+}_{(MeCN)}$ source in the presence of 5.0 mM TCNQ. In this case, reductive electrolysis at $E_{app} = 0.05$ V (prior to process I_{red}) for 180 s produced SEM images (Figure 11a) consisting of well-separated, randomly oriented, nanotube-like $Co[TCNQ]_2(H_2O)_2$ crystals. At a higher magnification (Figure 11b), most of these nanotubes are seen to exhibit outgrowths and have a defined hexagonal shape, at least at the tip, with a 300−500 nm diameter. The lengths of these nanotubes lie in the range of 5−8 μm. In contrast, SEM images (Figure 11c,d) of $Co[TCNQ]_2(H_2O)_2$ obtained at the potential of process I_{red} (−0.10 V) exhibit a far more compact film of much more densely packed, shorter crystals. The tips of most of these crystals are almost completely filled (Figure 11d). Thus, the difference in morphology encountered as a result of changing the identity of $Co^{2+}_{(MeCN)}$ counteranions and/or applied potential is probably attributable to the difference in the solubility and/or increased nucleation−growth rates of $Co[TCNQ]_2(H_2O)_2$ during the electrodeposition step.[9f]

(36) (a) Gunawardena, G.; Hills, G.; Montenegro, I.; Scharifker, B. R. *J. Electroanal. Chem.* **1982**, *138*, 225. (b) Scharifker, B. R.; Hills, G. *Electrochim. Acta.* **1983**, *28*, 879. (c) Scharifker, B. R.; Mostany, J. *J. Electroanal. Chem.* **1984**, *177*, 13. (d) Scharifker, B. R. *J. Electroanal. Chem.* **1998**, *458*, 253.

Scheme 2

$$TCNQ_{(MeCN)} + e^- \rightleftharpoons [TCNQ]^{\bullet-}_{(MeCN)}$$

$$2\,TCNQ_{(MeCN)} + 2\,[TCNQ]^{\bullet-}_{(MeCN)} \overset{Co^{2+}_{(MeCN)}}{\rightleftharpoons} \{[TCNQ_2]^{\bullet-}\text{--}Co^{2+}\text{--}[TCNQ_2]^{\bullet-}\}_{(surface\ confined)}$$

$$\{[TCNQ_2]^{\bullet-}\text{--}Co^{2+}\text{--}[TCNQ_2]^{\bullet-}\}_{(surface\ confined)} \overset{2e^-}{\underset{H_2O}{\rightleftharpoons}} \{Co[TCNQ]_2(H_2O)_2\}_{(film)} + 2\,[TCNQ]^{\bullet-}_{(MeCN)}$$

Finally, inspection of SEM images was also employed to probe the morphology of the electrocrystallized Co[TCNQ]$_2$-(H$_2$O)$_2$ at different $Co^{2+}_{(MeCN)}$:TCNQ ratios. As can be seen in Figure 12, reductive electrolysis experiments conducted at an applied potential of 0.05 V and deposition time of 180 s in acetonitrile (0.1 M [NBu$_4$][ClO$_4$]) containing 5.0 mM concentrations of both Co(NO$_3$)$_2$ and TCNQ (1:1 ratio) gave rise to crystal shapes (morphology) identical to those observed with a 1:2 ratio. XRD and EDAX data confirmed that the solid is crystalline and has the same composition as that obtained from a 1:2 ratio. Thus, changing the ratio of $Co^{2+}_{(MeCN)}$ to TCNQ does not change either the composition or the morphology of the electrocrystallized Co[TCNQ]$_2$(H$_2$O)$_2$.

In summary, SEM findings demonstrate that the nature (i.e., size, density, shape, orientation) of the electrodeposited Co-[TCNQ]$_2$(H$_2$O)$_2$ material is concentration and potential dependent and, with proper manipulation of the electrocrystallization parameters, the overall morphology can be precisely controlled to yield either nanowires or thin films. IR, Raman, XRD, TGA, and EDAX characterization of the electrocrystallized material considered in combination with SEM images implies that differences are confined to the morphology and not the composition of electrocrystallized Co[TCNQ]$_2$(H$_2$O)$_2$ solid.

V. Mechanistic Aspects of Co[TCNQ]$_2$(H$_2$O)$_2$ Electrocrystallization. Voltammetric, EQCM, galvanostatic, spectroscopic, diffraction and microscopic data all lead to the conclusion that the reduction of TCNQ to its $[TCNQ]^{\bullet-}$ monoanion radical in acetonitrile, in the presence of $Co^{2+}_{(MeCN)}$, induces the electrocrystallization of Co[TCNQ]$_2$(H$_2$O)$_2$ onto the electrode surface via at least two distinctly different, potential-dependent nucleation−growth mechanisms. The number of active nucleation sites generated is always likely to be proportional to the applied potential.[36b] However, electrocrystallization that commences at potentials prior to the onset of process I_{red} predominantly produces arrays of well-separated needle-shaped Co[TCNQ]$_2$(H$_2$O)$_2$ nanowires. Nucleation in this case is at randomly separated defect sites. When nucleation sites (most likely Co[TCNQ]$_2$) are generated at well-separated sites, rapid crystal growth into bulk solution of the identified Co[TCNQ]$_2$-(H$_2$O)$_2$ phase is probably faster than lateral growth across the surface and hence generates the morphology noted in the images in Figures 9 and 11a. This process is represented by Scheme 1.

On the other hand, SEM micrographs consisting of significantly more uniform and densely packed Co[TCNQ]$_2$(H$_2$O)$_2$ nanorods are produced when a potential more negative than process I_{red} is used for electrocrystallization. This suggests that a much larger number of more closely spaced nucleation sites are available for Co[TCNQ]$_2$(H$_2$O)$_2$ growth under these conditions.[36b] Since the faradaic current associated with process I_{red} is not a result of reduction of either $Co^{2+}_{(MeCN)}$ ions or bulk TCNQ, reduction of surface-confined TCNQ-containing molecules or metal stabilized dimers is expected to occur at more negative potentials than reduction of dissolved TCNQ.[37] Thus, process I_{red} is most likely to involve formation and reduction of a cobalt-stabilized anionic dimer, $\{(Co^{2+})([TCNQ_2]^{\bullet-})_2\}$, formed via a charge-transfer reaction between $[TCNQ]^{\bullet-}$ anion radical and neutral TCNQ,[38] as illustrated in Scheme 2. The fact that process I_{red} is not detected in the absence of $Co^{2+}_{(MeCN)}$ ions, and its marked potential dependence upon the $Co^{2+}_{(MeCN)}$ concentration, suggest that $Co^{2+}_{(MeCN)}$ ions play a key role in stabilizing the $[TCNQ_2]^{\bullet-}$ dimer anion. Furthermore, a mechanism involving reduction of $\{(Co^{2+})([TCNQ_2]^{\bullet-})_2\}$ is expected to generate a much higher density of nucleation sites than available by defect sites.

The existence of TCNQ-based anionic dimers such as the radical−substrate, $[TCNQ_2]^{\bullet-}$, or the radical−radical, $[TCNQ_2]^{2-}$, have been invoked under a range of conditions,[8a,15,37−39] and for the conceptually similar CuTCNQ analogue, reduction of the Cu-stabilized dimer anion, $\{(Cu^+)([TCNQ_2]^{\bullet-})\}$, was suggested as a possible means of formation of closely spaced nucleation sites, thereby generating arrays/films of closely spaced crystals in this system.[10e]

Less likely, the formation of Co[TCNQ]$_2$(H$_2$O)$_2$ via process I_{red} may involve reduction of an adsorbed sub-monolayer of TCNQ or its dimeric anion and not necessarily involve $Co^{2+}_{(MeCN)}$ stabilization. This assumption is based on the finding that the voltammetric characteristics of process I_{red} bear some resemblance to those reported for the solid−solid transformation of surface-confined water-insoluble TCNQ into Co[TCNQ]$_2$-(H$_2$O)$_2$ in aqueous media[18] according to eq 7. Thus, a sub-

$$2TCNQ_{(surface\ confined)} + Co^{2+}_{(aq)} + 2e^- \overset{H_2O}{\rightleftharpoons} \{Co[TCNQ]_2(H_2O)_2\}_{(s)} \quad (7)$$

molecular coverage of $[TCNQ_2]^{\bullet-}$ dimer anion would allow a uniform distribution of TCNQ to be achieved at the electrode surface and permit the occurrence of a process of the type described by eq 8, presumably via ingress and egress of $Co^{2+}_{(MeCN)}$ into the adsorbed film. As is the case with Scheme

$$2[TCNQ_2]^{\bullet-}_{(ads)} + Co^{2+}_{(MeCN)} + 2e^- \overset{H_2O}{\rightleftharpoons} \{Co[TCNQ]_2(H_2O)_2\}_{(s)} + 2[TCNQ]^{\bullet-} \quad (8)$$

2, numerous closely spaced nucleation sites for Co[TCNQ]$_2$-(H$_2$O)$_2$ crystal growth would be provided via this reaction (eq 8) to produce a densely packed film of Co[TCNQ]$_2$(H$_2$O)$_2$ crystals.

(37) Karimi, H.; Chambers, J. Q. *J. Electroanal. Chem.* **1987**, *217*, 313.
(38) (a) Lue, J.-M.; Rosokha, S. V.; Kochi, J. K. *J. Am. Chem. Soc.* **2003**, *125*, 12161 and references therein. (b) Kertesz, V.; Van Berkel, G. J. *J. Solid State Electrochem.* **2005**, *9*, 390.
(39) (a) Boyd, R. H.; Phillips, W. D. *J. Chem. Phys.* **1965**, *43*, 2927. (b) Bácskai, J.; Inzelt, G. *J. Electroanal. Chem.* **1991**, *310*, 379. (c) Faulques, E.; Leblanc, A.; Molinie, P.; Decoster, M.; Conan, F.; Sala-Pala, J. *J. Phys. Chem. B* **1997**, *101*, 1561. (d) Takahashi, K.; Kobayashi, K. *Tetrahedron Lett.* **1999**, *40*, 5349.

Despite the complexity associated with the deposition of Co[TCNQ]$_2$(H$_2$O)$_2$ onto the electrode surface, the stripping step is very rapid and, under conditions where thin films are formed, as confirmed by EQCM data (Figure 5), removes all solid from the surface, as illustrated by eq 9. However, when Co[TCNQ]$_2$-

$$[Co(TCNQ)_2(H_2O)_2]_{(s)} \xrightarrow[-2H_2O]{\text{stripping}} 2TCNQ + Co^{2+}{}_{(MeCN)} + 2e^- \quad (9)$$

(H$_2$O)$_2$ is electrocrystallized as long nanowires (at potentials prior to process I_{red}), stripping is not complete (Figure S2). Presumably, under these circumstances, some nanowires may become broken and hence be in poor electrical contact with the electrode surface; therefore, they are not amenable to full removal via electrochemical stripping.

Conclusions

The one-electron reduction of TCNQ to [TCNQ]$^{\bullet-}$ in acetonitrile in the presence of $Co^{2+}{}_{(MeCN)}$ ions leads to electrocrystallization of the sparingly soluble blue Co[TCNQ]$_2$(H$_2$O)$_2$ solid onto the working electrode surface. Two distinctly different, potential-dependent pathways are available for electrocrystallization that are governed by nucleation−growth kinetics, with the progressive 3-D growth stage being controlled by diffusion. SEM images reveal that the deposition potential plays a crucial role in controlling the shape, size, density, and uniformity of the electrocrystallized Co[TCNQ]$_2$(H$_2$O)$_2$ crystals. Deposition potentials more negative than the [TCNQ]$^{0/\bullet-}$ process, but prior to the onset of the sharp reduction process, I_{red} (typically between 0.1 and 0 V), lead to well-separated arrays of long, partially hollow nanowires/nanotubes, formed via the overall process $2[TCNQ]^{\bullet-}{}_{(MeCN)} + Co^{2+}{}_{(MeCN)} + 2H_2O \rightleftharpoons \{Co[TCNQ]_2(H_2O)_2\}_{(s)}$, where nucleation and growth occur at defect sites on the electrode surface. At potentials more negative than process I_{red}, but prior to the [TCNQ]$^{\bullet-/2-}$ process (between −0.05 and −0.15 V), a compact film of densely packed, uniformly oriented, hexagonal-shaped nanorod crystals is obtained. This is achieved, most likely, at a markedly increased number of nucleation sites created by direct reduction of a cobalt-stabilized $\{(Co^{2+})([TCNQ_2]^{\bullet-})_2\}$ dimeric anion.

Despite the marked dependence of Co[TCNQ]$_2$(H$_2$O)$_2$ morphology on deposition potential, time, and identity of $Co^{2+}{}_{(MeCN)}$ counteranion, as well as the concentration and ratio of both $Co^{2+}{}_{(MeCN)}$ and TCNQ, electrocrystallized Co[TCNQ]$_2$(H$_2$O)$_2$ is always crystalline, and differences in electrodeposited material are confined to the morphology and not to the phase or composition. Thus, this study provides promise for the electrochemical synthesis and fabrication of semiconducting/magnetic materials based on binary M[TCNQ]$_2$ (M = Mn, Fe, Co, Ni) with well-defined morphologies directly onto conducting or semiconducting electrode surfaces in a controlled manner for potential applications in nanoelectronic devices.

Acknowledgment. Financial support from the Australian Research Council is gratefully acknowledged. The authors also express their appreciation to Steven Pentinakis and John Ward at CSIRO Division of Manufacturing and Materials (CMMT) for technical assistance with the SEM instrumentation and Dr. Aaron K. Neufeld (Blue Scope Steel) for helpful discussions. The SR-GIXRD work was performed at the Australian National Beamline Facility (ANBF) with support from the Australian Synchrotron Research Program, which is funded by the Commonwealth of Australia under the Major National Research Facilities Program. We also thank Drs. Garry Foran and James Hester at the ANBF for support on the SR-GIXRD work.

Supporting Information Available: Figures S1−S7, showing voltammetric, EQCM, IR, TGA, and SEM images of electrocrystallized Co[TCNQ]$_2$(H$_2$O)$_2$. This material is available free of charge via the Internet at http://pubs.acs.org.

JA067219J